9-3-2013

# Flash heating of epoxy-based corrosion inhibitor thin films on aluminum substrates

Martin Dole

Martin Allen Dole
*Candidate*

Mechanical Engineering
*Department*

This thesis is approved, and it is acceptable in quality and form for publication:

*Approved by the Thesis Committee:*

Dr. Tariq Khraishi, Chairperson

Dr. Yu-Lin Shen

Dr. Brett Bedeaux

**FLASH HEATING OF EPOXY-BASED CORROSION INHIBITOR THIN FILMS ON ALUMINUM SUBSTRATES**

By

**MARTIN A. DOLE**

B.S., Mechanical Engineering, University of New Mexico, 2010

THESIS

Submitted in Partial Fulfillment of the
Requirements for the Degree of

Masters of Science
Mechanical Engineering

The University of New Mexico
Albuquerque, New Mexico

July 2013

# ACKNOWLEDGEMENTS

Embarking on the research and analysis for my thesis has been a learning experience and an adventure. All adventurers need a support system in order achieve a happy ending, and I have been lucky enough to have many people support me along the way with my adventure. First, I would like to thank the wonderful and helpful staff of the University of New Mexico Mechanical Engineering Department for helping me on more than one occasion access the essential resources to my project. Second, I am very grateful to Dr. Tariq Khraishi for his patience, understanding and tenacity to push me harder- ensuring that I succeeded in finishing my thesis. Third, I want to thank Dr. Brett Bedeaux for his trust in my work on this thesis and for keeping me focused on the main goal of my research. Dr. Bedeaux helped me by pointing me in the right direction of facilities and contacts that will undoubtedly be a part of my future career as an engineer. Fourth, I would like to acknowledge my boss Mr. Gregory Gross for his understanding and patience that allowed me to accomplish my research. Fifth, I feel a great deal of gratitude to Captain Jon Rowland. Captain Rowland had endless patience with me regarding equipment questions and programming issues. Without his help, the research for my thesis would have taken quite a bit longer. Finally, I would like to thank my son, Dustin Dole. Dustin has been my constant motivator to be a better man for the last six years and he himself is the main reason I push myself to succeed.

**FLASH HEATING OF EPOXY-BASED CORROSION INHIBITOR THIN FILMS ON ALUMINUM SUBSTRATES**

By

Martin A. Dole

B.S., Mechanical Engineering, University of New Mexico, 2010

M.S., Mechanical Engineering, University of New Mexico, 2013

## Abstract

The following research presents the experimental study of a transient heat load focused onto epoxy-polyamide primer which is used as a corrosion inhibitor coating. The thermal degradation initiation temperature of the epoxy polyamide film increased with increasing heating rates. This coating is a high solids epoxy primer manufactured by Deft Inc. A xenon flash lamp was focused to a one-inch diameter spot size on two types of aluminum substrates; AA2024-T4 and AA7075-T3. Edge effects were not considered for modeling. A ceramic firebrick insulated the aluminum coated disks to ensure that edge effects are negligible. The Forward Time Center Space (FTCS) model was developed to calculate the transient response for a flash loading of the thermal energy. Substrates were shown to have significant impact to energy absorption of the epoxy polyamide film, film surface temperature and absorbed energy.

# Table of Contents

## LIST OF FIGURES

## List of Tables

# 1 Introduction

Epoxy is used in combination with many hardening chemicals to enhance specific material properties. Adhesion, strength and corrosion resistance are some of the material properties that can be affected. Epoxy properties are similar, but the difference in two different hardeners could increase some material properties up to 20 times. To determine the epoxy type, an analysis of the material properties for the particular epoxy hardener is required. The thermal degradation is a property that has not been determined for most epoxies. Thermal degradation of epoxy occurs in three phases. The phase 1 degradation is complete when 10% mass loss is reached. Phase 1 thermal degradation causes the epoxy polyamide to have a darker pigmentation. Darker pigmentation increases the energy absorption coefficient of the epoxy. Phase 2 thermal degradation is complete when 50% mass loss is reached and has different byproducts. Phase 3 thermal degradation is complete when roughly 75% mass loss is achieved. The final mass loss may vary based on the hardener combined with epoxy. All of these phases have byproducts that can damage the materials they are applied to. Research has been done to determine mechanical and chemical responses of epoxies in pure and matrix forms (e.g. fiberglass). When investigating the thermal response of epoxies, it has been found that the epoxy degrade differently with respect to the heating rate. The commonly used heating rate to determine epoxy material properties at elevated temperatures is 5°C/min (1:5). Many experiments using lasers use a black overlay on coupons to ensure energy was absorbed (1). Research using higher heat rates included investigation of ablative effects and examining epoxy pellets of different types

consisting mostly of diglycidyl ether of bisphenol A (DGEBA) epoxy resins (7:9). The following research was performed to monitor and study color change, peeling or any other damage to indicate initiation of phase 1 degradation.

## 1.1 History

Epoxy polyamide primers are used in a variety of applications including as a corrosion inhibition. The epoxy polyamide primer offers corrosion resistance that is superior to many other materials available. However, it has not been evaluated for thermal degradation or for its material properties. While the density of epoxy polyamide is reported by many manufacturers, other material properties remain unknown such as thermal conductivity, specific heat capacity and degradation information. The transient response of the epoxy polyamide is important to understand because phase 1 degradation byproducts are unknown and other epoxy compounds are known to have damaging byproducts (2). A transient analysis of the incident thermal loading is required to determine how the epoxy polyamide degrades under varied heating rates.

Transient state heat transfer models are often complicated and require computer power beyond that of commercially available computers. Analytically unsolvable boundary conditions require numerical methods to determine the response of materials through modeling. Transient state experiments are hard to design because data is hard to measure. Transient state heating phenomena are easy to recreate. Thermocouples are generally used in large bars or other geometry with well-defined heat sources and heat sinks to provide adequate data for analysis and understanding of the material response to the thermal loading. Thermocouples are too invasive for measuring the transient state of thin films

due to the heat capacity of the thermocouple. The high heat conductivity can absorb energy intended for epoxy polyamide film and create a cold spot creating another mechanism of heat transfer to cool the films surface. The thermocouple's heat conductivity has a significant effect on data, especially at moderate (~50$\frac{W}{mK}$) and larger values. Epoxies thermal conductivity ranges from 0.1 to 4$\frac{W}{mK}$ (3) depending on the hardener used. The higher conductivity of the thermal couple would create a cooler region on the film surface removing the incident heat loading.

### 1.2 Theory and Governing Equations

Transient state heat transfer is defined by the partial differential equation derived from the conservation of energy. Energy density is defined as $e(x,t)$. A differential volume is added to obtain the total heat energy $E(x,t) = e(x,t)Adx$.

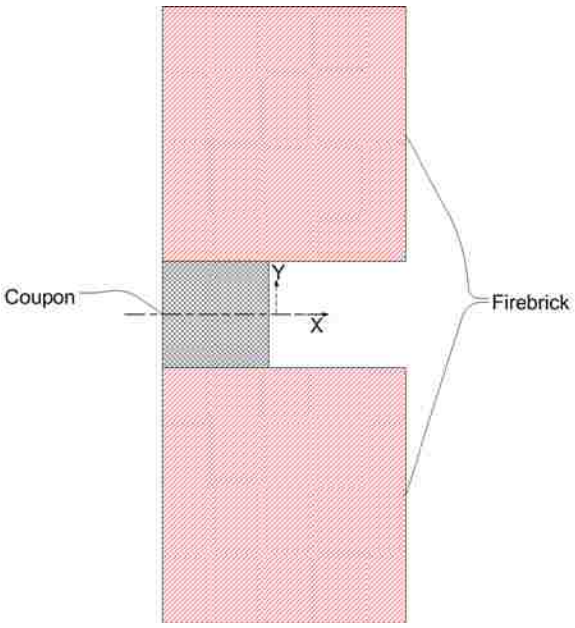


**Figure 1-1: Schematic of the Coupon Inside the Insulating Firebrick**

The fundamental heat flow process with constant volume combined with the conservation of energy is $\frac{\partial}{\partial t}[e(x,t)Adx]$. Adding heat sources of the material to this balance along with boundary conditions and external heat sources determine the change in heat energy with respect to time. Generalized heat flux flowing over the surface area of any boundary is

defined as $\Phi(x,t)$. Generalized heat source per volume per unit time is Q(x,t). The boundary conditions are non-zero at x=0 and x=L, because the sides of the coupons were insulated as shown in Figure 1-1. The boundary conditions, $\frac{\partial \Phi}{\partial x}$, and internal heat sources, $Q$, are added to the energy balance, and differentiated with respect to time, giving $\frac{\partial e}{\partial t}Adx = -A\frac{\partial \Phi}{\partial x} + QAdx$. There are no internal heat sources in the volume of this experiment, therefore Q=0. There is a source at the boundary, a flux $\alpha_{Ab}\dot{q}$ that is the xenon flash lamp's energy absorbed by the coupon. Here the $\alpha_{Ab}$ term is the absorptivity of the epoxy polyamide film and $\dot{q}$ is the incident power .The $\alpha_{Ab}\dot{q}$ term is a part of the $-\frac{\partial \Phi}{\partial x}$ boundary condition term (not a source inside the material, and is not included in the Q term). To obtain temperature from this equation, the energy and temperature relationship is substituted into the conservation of energy giving $E(x,t) = c\,(x)\rho(x)Adx\frac{\partial T}{\partial t} = -A\frac{\partial \Phi}{\partial x}$. The boundary condition is still not well-defined in this form. Fourier's Law is required to relate the heat conservation equation to the material properties using the following substitution $\Phi = -K_0\frac{\partial T}{\partial x}$, where $K_0$ is the thermal conductivity of the material. $K_0$ is also denoted as 'k' and 'k' is used as thermal conductivity of materials throughout the rest of this research. The $\Phi = -k\frac{\partial T}{\partial x}$ term accounts for surface boundary conditions that rely on material properties and environmental factors. Boundary conditions include heat transfer mechanisms for convection and radiation and external heat sources and sinks. The convection and radiation are also represented by Newton's Law of Cooling and the variable Φ by

$$\Phi = -h\left(T_\infty - T_{Surface}\right) - \varepsilon\sigma\left(T_\infty^4 - T_{Surface}^4\right) - \alpha_{Ab}\dot{q} = -k\frac{\partial T}{\partial x}.$$

Here, h is the convection coefficient, ε is the material emissivity; σ is the Stefan-Boltzmann constant and $\alpha_{Ab}\dot{q}$ is the energy absorbed from the flash by the epoxy polyamide. These specific boundaries and the source can be seen in Figure 1-2, where the back surface shows negligible convection that is discussed in the results section. The aluminum was not exposed to free flowing air on the non-coated backside, but there is still convection. The true amount of convection at the back surface is not easily calculated and is assumed to

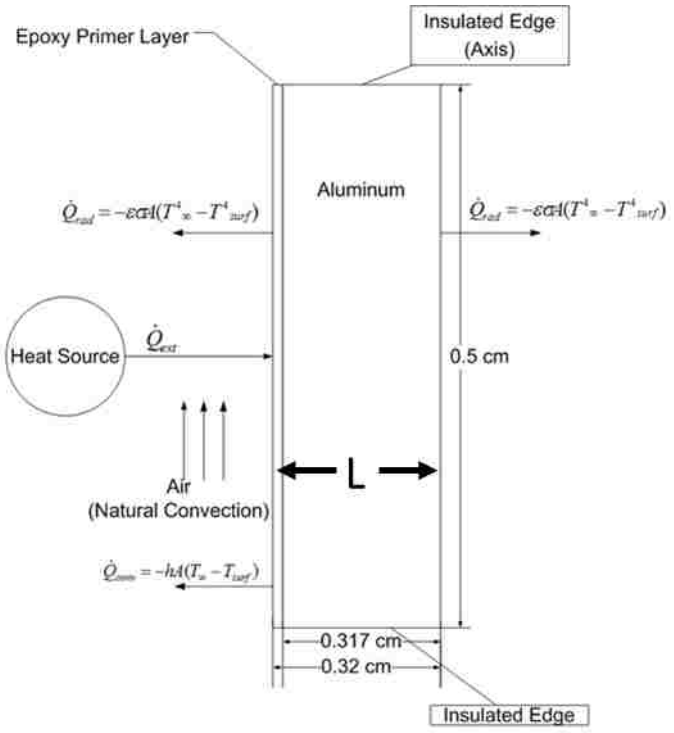


**Figure 1-2: Coupon Thermal Loading Diagram**

act as a vertical plane for the purpose of calculations required to determine the convective coefficient described later. The samples, more commonly referred to as coupons have thickness L and flash starts at t=0. This gives the partial differential equation form of the heat conducted through the flashed coupons as:

Equation: $$\rho(x)c(x)Adx\frac{\partial T}{\partial t} = kA\frac{\partial^2 T}{\partial x^2} - A\frac{\partial \Phi}{\partial x}$$

B.C.: $$\Phi(0,t) = -h\left(T_\infty - T_{Surface}\right) - \varepsilon_{ep}\sigma\left(T_\infty^4 - T_{Surface}^4\right) - \alpha_{Ab}\dot{q}$$

$$\Phi(L,t) = -h\left(T_\infty - T_{Surface}\right) - \varepsilon_{Al}\sigma\left(T_\infty^4 - T_{Surface}^4\right)$$

I.C.: $T(0,t) = T_0$

To determine the convection coefficient for the coupons, the properties for natural convection on a vertical plane were used to approximate the value of the convection coefficient. This requires the use of air properties at a film temperature, which can be taken as the average of the surface temperature and the environmental temperature. To determine the convection coefficient the Nusselt number is calculated and multiplied by the thermal conductivity of air and divided by the diameter of the coupon. Rayleigh (Ra), Grashof (Gr), and Prandtl (Pr) numbers are required for this calculation. The Prandtl number is the ratio of molecular diffusivity of momentum and the molecular diffusivity of heat given by $= \frac{v}{\alpha}$ ; where $\alpha$ is the thermal diffusivity of air and $v$ is the kinematic viscosity of air. The values of the Prandtl number are tabulated based on dependence of pressure and temperature. The air properties are taken at atmospheric pressure and the average temperature of air and primer surface for the following: Prandtl number (Pr), kinematic viscosity (v), the thermal expansion coefficient ($\beta$) and gravity (g). Gravity is required for the calculation of the natural convection coefficient as it hinders the air flowing up the surface of the coupons and has a value of $9.801\frac{m}{s^2}$. Material properties of air at the film temperature are provided in Table 1-1.

**Table 1-1: Material Properties of Air at the Film Temperature Taken as an Average of 300k for the Surroundings of 300K and Surface Temperature up to 500K**

| | Average Temperature of Air and Epoxy Primer [K] | | | | | |
|---|---|---|---|---|---|---|
| | 313.15 | 333.15 | 353.15 | 373.15 | 393.15 | 413.15 |
| Thermal Expansion (β) [1/K] | 0.0032 | 0.003 | 0.00283 | 0.00268 | 0.00255 | 0.00243 |
| Thermal Conductivity (k) $\left[\frac{W}{mK}\right]$ | 0.0271 | 0.0285 | 0.0299 | 0.0314 | 0.0328 | 0.0343 |
| Kinematic Viscosity (v) $\left[\frac{m^2}{s}\right]$ | 1.70E-05 | 1.89E-05 | 2.09E-05 | 2.31E-05 | 2.52E-05 | 2.76E-05 |
| Prandtl Number | 0.711 | 0.709 | 0.708 | 0.703 | 0.700 | 0.695 |

The Grashof number is the dimensionless ratio of buoyancy and viscous forces acting on a fluid. The Grashof number was calculated using the relation, $Gr_L = \frac{g\beta(T_S - T_\infty)D^3}{v^2}$, here D is the diameter of the coupon. This relation is based on the derivation of the Grashof number for a vertical plane. The Rayleigh number is ratio of buoyant forces and viscous forces times the ratio of momentum diffusivity and thermal diffusivity. The Rayleigh number is a function of the Grashof and Prandtl number through the following relation $Ra_L = GrPr$. The relation of Rayleigh and Nusselt for a flat vertical plane and the determination of convection from the Nusselt number is given by:

$$Nu = \left\{ 0.825 + \frac{0.387 Ra_L^{1/6}}{\left[1 + (0.492/Pr)^{\frac{9}{16}}\right]^{\frac{8}{27}}} \right\}^2 \text{ and } h = k\frac{Nu}{D}.$$

**Table 1-2: Calculated Values Used for the Calculation of the Convective Coefficient**

| | Average Temperature of Air and Epoxy Primer [K] | | | | | |
|---|---|---|---|---|---|---|
| | 313.15 | 333.15 | 353.15 | 373.15 | 393.15 | 413.15 |
| Grashof | 1.79E+05 | 3.41E+05 | 4.20E+05 | 4.52E+05 | 4.57E+05 | 4.44E+05 |
| Rayleigh | 1.27E+05 | 2.42E+05 | 2.98E+05 | 3.18E+05 | 3.20E+05 | 3.08E+05 |
| Nusselt | 9.75 | 11.45 | 12.07 | 12.26 | 12.28 | 12.16 |
| Convection Coefficient $\left[\frac{W}{m^2K}\right]$ | 5.28 | 6.53 | 7.22 | 7.70 | 8.06 | 8.34 |

Calculation of quantities required for the determination of the convective coefficients at specified temperatures, are reported in Table 1-2. The calculation of the average value of the convective coefficient used the assumption that the coupons' front surface temperatures did not exceed 500k and the rear surface temperatures did not exceed 400k. The average value for the convection coefficient of the front surface of the coupons is $h = 7.2\ \left[\frac{W}{m^2K}\right]$. Using the average of the first three convective coefficient values from Table 1-2 the convective coefficient for the back surface of the coupon is $h = 6.3\left[\frac{W}{m^2K}\right]$.

A Forward Time Center Space (FTCS) finite difference model was developed to predict temperature and energy absorbed for each the measured incident energies. The heat equation needs to have the volume added and becomes $c(x)\rho(x)Adx\frac{\partial T}{\partial t} = -A\frac{\partial \Phi}{\partial x}$. This is done to have a specified mass of material the heat flows through. The heat flows through an area into the mass, and the volume is discretized into "N" elements each $\Delta x$ thick. The discretized equation for each node is given as:

$$\rho A\Delta x C_p \frac{T_n^{i+1}+T_n^i}{\Delta t} = kA\frac{T_{n-1}^i+T_{n+1}^i-2T_n^i}{\Delta x} - A\frac{\partial \Phi}{\partial x}.$$

The discretized heat equation was applied to the respective materials of the node "n" at the time step "i". The convection, radiation and external sources are in the $-\frac{\partial \Phi}{\partial x}$ term. Now the equation can be rearranged as:

$$T_n^{i+1} = \frac{k\Delta t}{\rho C_p}\frac{T_{n-1}^i + T_{n+1}^i - 2T_n^i}{\Delta x^2} - \frac{\Delta t}{\rho C_p \Delta x}\frac{\partial \Phi}{\partial x} + T_n^i \ ,$$

The material properties are assumed constant. Heat is assumed to flow in the x direction only. The heating of the epoxy surface exposed to the flash at node 1 was discretized as shown in Figure 1-3. The interior nodes have conduction on both sides, except for the last node for the back surface, which incorporates convection and radiation conditions. The $-\frac{\partial \Phi}{\partial x}$ term for the front surface node includes the boundary conditions for convection, radiation, and the incident flux from the xenon flash lamp. The $-\frac{\partial \Phi}{\partial x}$ term for node 1 becomes $2\tau_{ep}\left\{\frac{\Delta x}{k_{ep}}\left[\alpha_{Ab}q - h_F\left(T_1^i - T_\infty\right) - \varepsilon_F\sigma\left(T_1^{i^4} - T_\infty^4\right)\right]\right\}$, from the boundary fluxes. Applying the boundary conditions and conduction to node 1, the discretized heat equation becomes:

$$T_1^{i+1} = 2\tau_{ep}\left\{\frac{\Delta x}{k_{ep}}\left[\alpha_{Ab}q - h_F\left(T_1^i - T_\infty\right) - \varepsilon_F\sigma\left(T_1^{i^4} - T_\infty^4\right)\right] + T_2^i - T_1^i\right\} + T_1^i.$$

Here $\tau = \frac{k\Delta t}{\Delta x^2 \rho C_p}$ and is dependent upon the properties of epoxy, k is the thermal conductivity, $\Delta x$ is the element length. $h_F$ is the convection coefficient applied to the front surface. $\sigma$ is the Stephan-Boltzmann constant and $\varepsilon_F$ is the emissivity coefficient applied to the front surface for the radiation boundary condition. Interior nodes are only acted on by conduction therefore $-\frac{\partial \Phi}{\partial x} = 0$ .The interior nodes temperature is given by:

$$T_n^{i+1} = \tau\left(T_{n-1}^i + T_{n+1}^i - 2T_n^i\right) + T_n^i \ .$$

$\tau$ is defined as above, but node properties are determined from the properties of aluminum for nodes in the aluminum substrate region. Epoxy polyamide properties for nodes located in the epoxy polyamide primer region. The interface

node has heat conduction from the epoxy polyamide node next to it and the aluminum node next to it. The calculation for the interface node required the inclusion of all properties and the difference in node size had to be accounted for in the discretized heat equation. The interface node temperature is defined as:

$$T_{int}^{i+1} = \left[ \frac{\frac{k_{ep}}{\Delta x_{ep}} T_{int-1}^{i} + \frac{k_{Al}}{\Delta x_{Al}} T_{int+1}^{i} - \left( \frac{k_{ep}}{\Delta x_{ep}} + \frac{k_{Al}}{\Delta x_{Al}} \right) T_{int}^{i}}{\rho_{ep} C_{p_{ep}} \Delta x_{ep} + \rho_{Al} C_{p_{Al}} \Delta x_{Al}} \right] + T_{int}^{i} .$$

The last node subject to the boundary conditions, $-\frac{\partial \Phi}{\partial x}$, are defined similarly to the front surface without the incident flux term. The $-\frac{\partial \Phi}{\partial x}$ term for the last "N+1"th node becomes $2\tau_{Al}\left\{\frac{\Delta x}{k_{Al}}\left[-h_R\left(T_{N+1}^{i} - T_\infty\right) - \varepsilon_R \sigma\left(T_{N+1}^{i^4} - T_\infty^4\right)\right]\right\}$ for the back surface after applying the convection and radiation conditions. The substitution of the $-\frac{\partial \Phi}{\partial x}$ term into the last nodes discretized heat equation gives:

$$T_{N+1}^{i+1} = 2\tau_{Al}\left\{\frac{\Delta x}{k_{Al}}\left[-h_R\left(T_{N+1}^{i} - T_\infty\right) - \varepsilon_R \sigma\left(T_{N+1}^{i^4} - T_\infty^4\right)\right] + T_N^i - T_{N+1}^i\right\} + T_{N+1}^i.$$

The discretized coupon has N elements and N+1 nodes that the discretized heat equation is applied to. These equations applied to the proper nodes yield a time history of the temperature at each node as long as $\tau < 0.5$ for both aluminum substrate and epoxy polyamide primer. If the condition of the Fourier Constant $\tau < 0.5$ is not maintained, the system of equations becomes unstable.

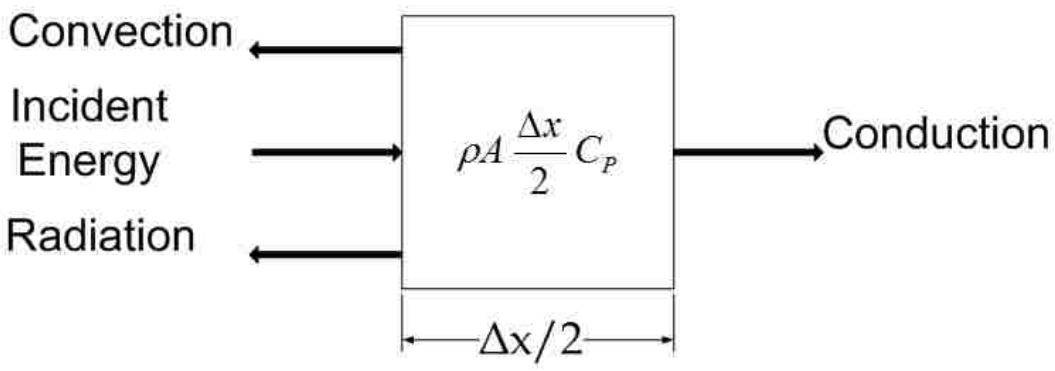


**Figure 1-3: First Node for FTSC Model with Boundary Conditions**

## 1.3 Goals of Study

The purpose of this research is to determine the time and flux dependence required for phase 1 degradation of epoxy polyamide using epoxy polyamide-coated aluminum coupons. The substrate effects on the epoxy polyamide were also evaluated. The heat loading consisted of an intensified solar radiation to an epoxy polyamide primer conforming to the MIL-PRF-23377 (4) and MIL-DTL-81706 (5). The epoxy polyamide is subjected to thermal loads in the range of $10\frac{W}{cm^2}$ and $50\frac{W}{cm^2}$ to determine the time-dependent response of the epoxy polyamide primer. Modeling the temperature response of the epoxy polyamide surface required a parametric analysis to determine the substrate effects. Substrates affected the surface temperature of the epoxy polyamide primer and how the heat flowed through the coupon.

# 2 Earlier Work

## 2.1 Pulsed Laser Research

Research efforts have delineated laser ablation and laser annealing heat loads (6) with applications in nano-imprinting processes. Ablative and annealing heating are different transient responses. The way the heat transfer occurs requires modeling to determine how the heated material reacts. The ablative energy required was determined to be around 1 $\left[\frac{J}{cm^2}\right]$ after 1 ns. This requires an energy deposition rate of 1 $\frac{GW}{cm^2}$ at the minimum to achieve ablation and resulting molten phase of the copper. The temperature profiles of copper are shown in Figure 2-1. The horizontal lines indicate the solidification of the surrounding copper substrate from the ablated region. The experimental setup of this ablation research was used to assist in experimental design of the epoxy polyamide applied to this specific research.

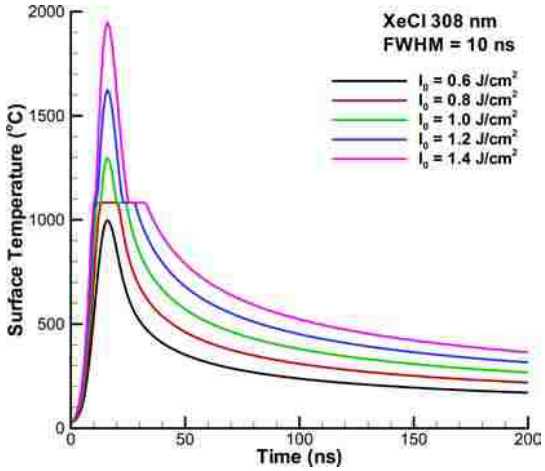


**Figure 2-1: Temperature Profile of the Copper Substrate**

A similar set of experiments used silver-nickel coatings on copper substrates. These coatings were highly reflective, which necessitated a black overlay to absorb the energy (7). The silver-nickel coatings used in the

experiment were exposed to a much higher energy on a smaller spot size of the laser for a shorter period. The laser was 6kW on a 1.8mm spot size resulting in a power to area, in sq.cm, of ~240,000 $\frac{W}{cm^2}$. The duration of laser exposure was between 1.5 and 3.5 ms and had a total incident energy of 9 to 21 $\frac{J}{cm^2}$. Bubbles trapped in the molten coatings resulted in crack formation on the surfaces of the silver-nickel coatings after cooling. A separate research effort trying to model ablation of zirconia coatings on lead alumina substrates used a 150fs pulse, over a 27μm diameter spot size. Energy disposition was varied to determine the ablation energy required for the zirconia coating. The ablation point found was 1.61$\frac{J}{cm^2}$ (1), from the heat flux rate of 1.07$* 10^{13}\frac{W}{cm^2}$. The thermal loading of this magnitude is achievable only because the focus of the laser beam came to a 27μm diameter spot size. This high flux rate was necessary to ablate the surface of the zirconia coating on the Lead-Aluminum substrate. The previous research efforts showed the effect of substrate material on the coatings' energy absorption which determined the need for this research to model the aluminum substrates effect on the epoxy polyamide primer.

The Naval Research Laboratory conducted ablation experiments using a 15 kW laser with epoxy graphite composites to determine epoxy ablation response (8). The results of ablation showed a degradation temperature similar to a published epoxy degradation temperature (420°C) (3). However, this research project was only concerned with the ablation of the epoxy resin matrix. Material properties of the epoxy graphite matrix with defined epoxy degradation are shown in Figure 2-2. The epoxy ablation research used energy over area

values ranging up to $3\frac{kW}{cm^2}$. Energy deposition at this rate was required to determine epoxy ablation characteristics. The absorption coefficient of the epoxy graphite composite approached 1 as the epoxy charred and ablated, leaving graphite to absorb the thermal energy.

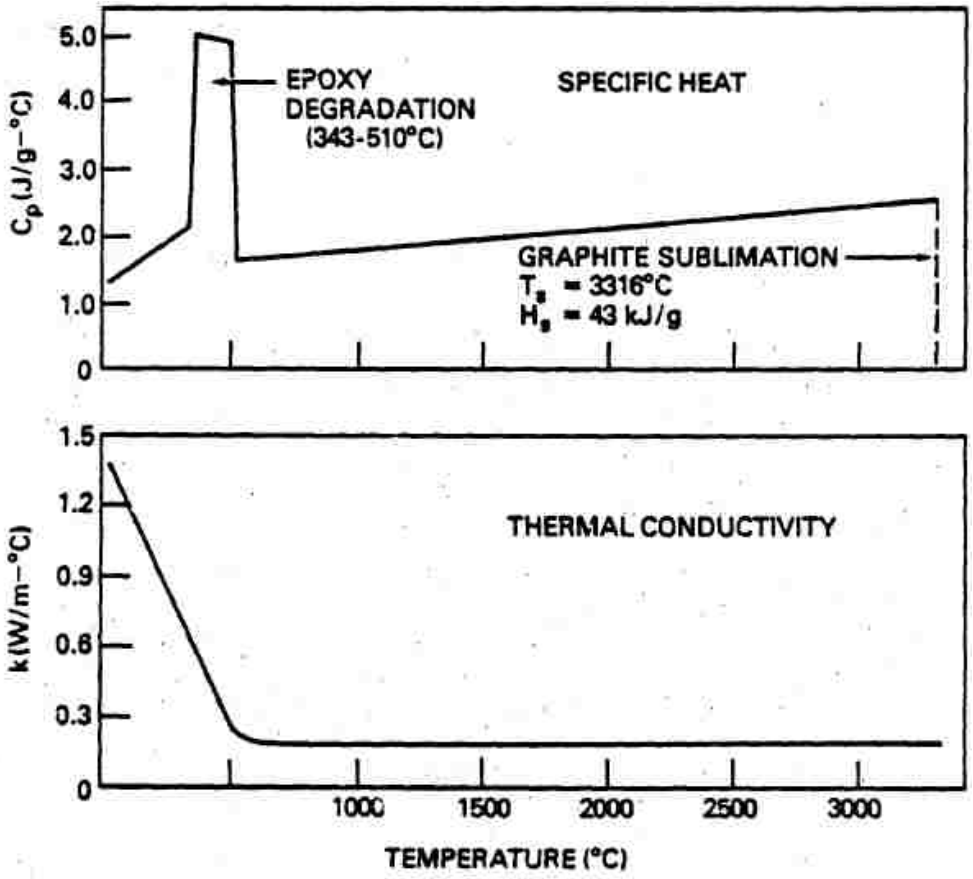


**Figure 2-2: Epoxy Properties at different temperatures provided by the Naval Research Laboratory Griffis et al.**

## 2.2 Paint / Primer Specific Research

Rosu et al. studied how heating rates affected the degradation phases of Epoxy maleate of bisphenol A. This epoxy was thermally heated from 25°C to 500°C to achieve complete epoxy degradation. The epoxy degraded in three phases at different temperatures that were dependent on temperature rates. The heating rates of 5.5, 9.0, 12.0 and 16.0°C/min were performed to find the

initiation of the three degradation phase temperatures (9). The different heating rates resulted in the lower end of the phase I degradation starting between 79°C and 83°C at heating rates of 5.5°C/min and 16.0°C/minute. Heating at these rates showed a trend as the incident heat increased, the phase I initiation temperature increased, along with the initiation temperature of the phase II degradation. The total temperature profile of the epoxy pellets can be seen in Figure 2-3. Activation Energy of 49$\left[\frac{kJ}{mol}\right]$ was found to be constant for all thermal loading rates. The research showed the heating rate dependence of epoxy is determined by the activation energy of the epoxy, which was examined in this work for the epoxy polyamide coated aluminum coupons.

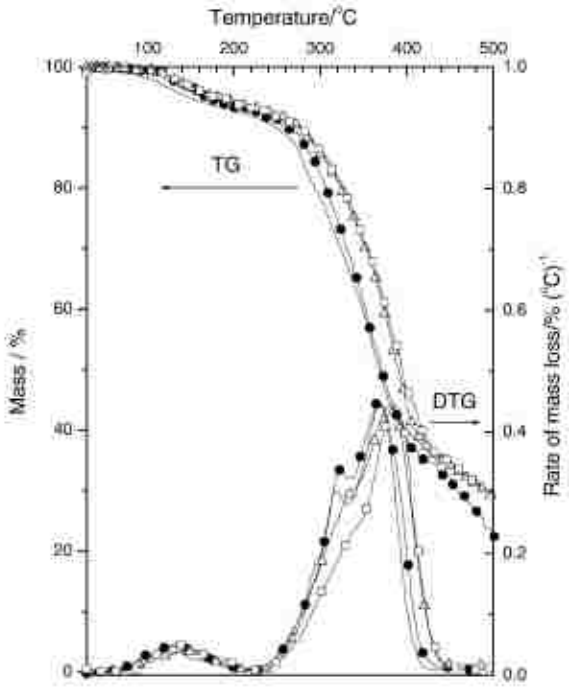


**Figure 2-3: Temperature Profile of Epoxy Maleate of Bisphenol A degradation, provided by Rosu et al.**

Research was performed by Kim et al. to determine paint damage effects of painted surfaces submerged in water. The surfaces were coated with white,

black, and silver pigmented paint (10). The experiment for submerging the coated metals while heating them used a carbon dioxide laser rated at 250 W with a 9 mm spot diameter resulting in a power over area value of 393$\frac{W}{cm^2}$. The research compared damage done to coated metals submerged in water to dry painted metals. Temperatures were recorded on the back surface through use of a thermocouple. The uncoated metal did not reach as high of a temperature as the coated samples, even though the temperature was measured on the back surface. The results indicated that the dry painted metal absorbed more than wet painted metal, which absorbed more than dry uncoated metal as shown in Figure 2-4. Analysis showed the energy absorption dependence of the substrates increased when a coating was added.

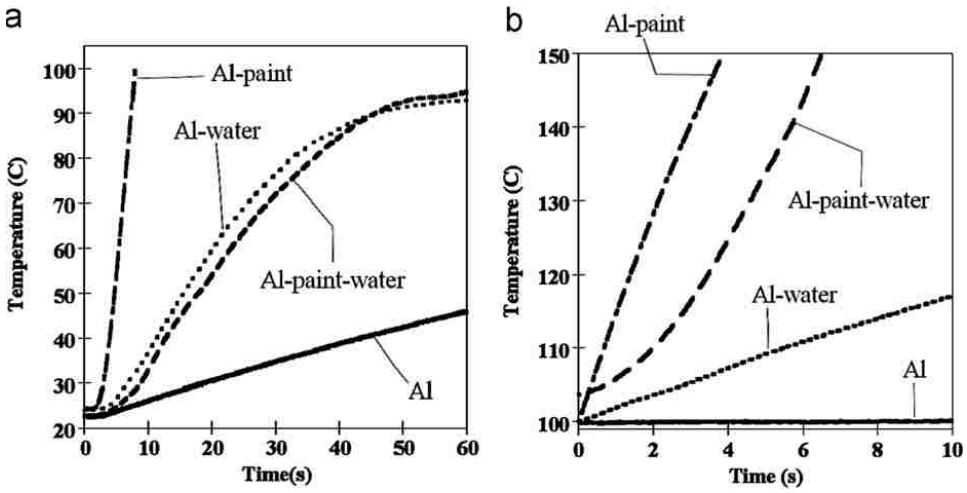


**Figure 2-4: Aluminum Back Surface Response to $CO_2$ 0.39kW/cm$^2$ Laser Courtesy of Y.H. Kim et al.**

Epoxy resins were used in conjunction with dangerous toxic materials to ensure components did not catch on fire. Some of these compounds have been banned or limited. These bans and limitations have led to a need to identify different epoxy matrices or alter epoxy compounds to provide this critical fire

protection function (11). In particular flammability appears to be effected by altering the compounding components. The chosen epoxy was Polyepoxyphenylsilsesquioxane (PEPSQ) epoxy and degradation temperature was determined for the heating rates of 5, 10 20, and 40°C/min (11). Degradation was initiated at about 250°C for the epoxy pellets. The activation energy was calculated to be roughly 40$\left[\frac{kJ}{mol}\right]$. The results showed that the degradation dependence on heating rate was a function of energy for degradation.

None of the previously discussed research considered an epoxy polyamide coating on an aluminum substrate. Damage to epoxy polyamide coating mounted on aluminum substrates could include thermal degradation, which includes increased absorption of energy, peeling, spalling, or de-bonding. The known epoxy polyamide properties are the corrosion resistance and cured density. Specific heat capacity, conductivity and degradation temperatures remain unknown. This research determined phase I degradation initiation of epoxy polyamide from both temperature and absorbed energy.

### 2.3 Finite Element Method Development

Many methods have been developed to solve complex real world problems. One method is the Forward Time Center Spaced (FTCS) finite-difference method, which uses finite elements and simple boundary conditions. This includes conduction, convection and radiation for discrete material volumes (12). To ensure stability, the Fourier Constant $\tau$ must be less than 0.5 and the thin epoxy layer requires a Δx that is to the order of $10^{-6}$ meters, necessitating a time step of $10^{-6}$ seconds or the solution becomes unstable. Another method

that can be used to model the coupons' transient heat transfer response is the semi-discrete Galerkin method. The semi-discrete Galerkin method uses the partial differential form of the heat equation with a defined residual left in the solution, which is the cause of error due to discretization. Increasing the number of elements decreases the model's analytical error (13). To ensure minimal errors are present methods used in modeling are chosen based on the problems complexity, understanding of the individual methods, industry standards, and applications. Research and experimentation are required to ensure that the modeling procedure selected is appropriate for the specified conditions of the problem.

# 3 Experimental Setup

## 3.1 Experimental Requirements

The experimental design for epoxy polyamide degradation has many constraints and requirements that influenced the overall experimental setup. Transient state heat transfer experiments require a high intensity thermal source with little or no start-up time, scales, video cameras and thermal cameras. The high intensity heat source requires a non-contact heat source such as a laser. Metal or ceramic contacts would have to be preheated and flat to ensure that the correct wattage was being delivered. Temperature measurements are also difficult to determine for the epoxy polyamide layer using solid heating sources because measurements could not be performed on the epoxy surface. The interface of a solid heating element and coupon would create additional variability in the experiment due to surface roughness. A laser heat source negates any interface resistance. This allows for temperature measurements to be taken at the epoxy primer surface. Two of the lasers that were considered for this experiment were a high intensity infrared (IR) laser and a xenon flash lamp. The cost of the IR laser was determined to be too high and had limited availability. The xenon flash lamp's was available without a fee but required travel. The xenon flash lamp that was used for this experiment was located at the Air Force Institute of Technology (AFIT) Xenon Thermal Simulator Lab at Wright-Patterson Air Force Base near Dayton, OH.

Contact with the epoxy primer surface could not be used as a method of measuring the temperature of the epoxy film. The probes would interact with the

xenon flash lamp beam and absorb the energy intended for the epoxy primer surface. Probe contact would also create a source of heat transfer- to and from- the epoxy primer, further compromising results. Probes record only one data point- not a collection of data points across the surface to determine if there were edge effects. Thermal cameras were used to overcome the need to remotely interact with the epoxy primer surface, and back surface of the aluminum substrate.

To meet experimental requirements, two thermal cameras manufactured by FLIR with a resolution of 120x640 pixels were used for this research. The FLIR thermal cameras have the capability of recording many temperature points for the epoxy and substrate surfaces. Proper focusing of the FLIR cameras on the coupon required that the camera in the front had to be about 10 inches away from coupon, while the camera in the back had to be about 2 ft. away to accurately capture the boundary of the coupon and firebrick. The camera in the front also had to be offset about 45° from coupons' axis, due to space taken up by the xenon flash lamp and to avoid beam interaction. The camera in the front had over 70 points focused on the coupon even with this off set. The thermal camera in the back was oriented nearly orthogonal to the coupon. The camera could view the back surface of the coupon with close to 50 points of data, depending on focus. The thermal camera in the back was harder to focus when the firebrick was cool because the firebrick and coupon temperatures were similar.

**Figure 3-1: Burnt Epoxy Film Used for Experimental Verification and Position of recording Equipment**

Control of the xenon flash lamp was an issue because control boxes were out of reach making it difficult to open and close the shutter on the xenon flash lamp. The control box for the shutter of the xenon flash lamp needed to be accessed in order to stop burning the coupons before initiating phase 2 degradation of epoxy primer. Using a Compaq computer connected to the control boxes, and MatLab to communicate with power and control boxes to overcome these issues. MatLab was used to set the xenon flash lamp power and the keyboard was used to open and close the shutter. The fore mentioned system did not assist in determining the instant that smoke occurred on the primer. However, this did enable the shutter to close before phase 1 degradation was complete.

Experimental setup was verified using a 2024-T4 aluminum substrate coupon, ensuring beam focus and proper epoxy-beam alignment. Insulating the edges of the coupons was deemed necessary, after several runs using a single coupon (not included in the data set), shown in Figure 3-1. These flashes determined that even though the beam is larger than the coupon, insulation of the coupon is required to negate edge effects. The need for insulation arose from several physical constraints. First, the coupon was in contact with a metal

bracket, adding a mechanism for heat transfer to cool the epoxy polyamide coated aluminum substrate. Second, the amount of energy lost to convection from the sides of the coupon is unknown and could have impact on the heating rate of the epoxy primer. To insulate the coupon, a material with a low conductivity and a high interface resistant surface was required. Firebricks have a low conductivity combined with a high porosity. Therefore, firebricks reduced the edge effects on the coupon. Firebrick combined with coupons that were cut much smaller than the beam's spot size minimized the variation of the beam intensity over the coupon surface and reduced edge effects to negligible values. The firebrick also insulated the back surface of the coupon from convective losses and limited air circulation across the back of the coupon. After the coupon was inserted into the firebrick, the same single AA2024-T3 coupon also verified negligible heat transfer from the firebrick to the aluminum-epoxy coupons.

### 3.2 Representative Aircraft Control Surface

The primer that was used for this experiment is DEFT Inc.'s high solids epoxy primer that has been used in many corrosion inhibiting applications. A facility with the capability to perform this deposition was needed in order to apply the epoxy primer between 0.6-0.9 mils thick to the aluminum substrates (4). The epoxy primer deposition and curing for this experiment occurred at Hill AFB in Ogden, Utah in accordance with MIL-PRF-23377K. The aluminum substrates chosen were AA2024–T4 and AA 7075–T3. Damage due to heating of the aluminum substrates is not within the scope of this experiment. Thickness and tolerance information is reported for the epoxy polyamide primer and the aluminum substrates in Table 3-1 (4) (14).

**Table 3-1: Thickness and Tolerance for Epoxy Primer and Aluminum**

| | Epoxy Primer | | Aluminum AA2024–T3 | | Aluminum AA7075–T6 | |
|---|---|---|---|---|---|---|
| Thickness | 23 µm | 0.0009 in | 3.175mm | 0.125 in | 4.826mm | 0.19 in |
| Tolerance | +0 µm<br>-8 µm | +0.0000 in<br>-0.0003 in | ±0.089mm | ±0.0035 in | ±0.178mm | ±0.007 in |

Coupons were cut using a water jet after the epoxy was applied. In total, 150 coupons were cut into 1cm diameter disks. Of the cut coupons, 129 were used in this research and 123 had useable thermal camera data. To avoid damage during transport, coupons cut were left attached to the aluminum sheets. Pushing on the back surface of the aluminum ensured that no damage occurred to the epoxy polyamide primer during removal. To further ensure the safety of the coupons during removal from the aluminum sheets a hand and paper were placed underneath the coupons. Nitrile gloves were used in the handling of the primer coated aluminum coupons to prevent contamination before heating. Coupons force fitted into the firebrick did not cause damage to the coupon because the firebrick easily broke away to allow the coupons to be inserted. After several coupons had been inserted and removed, the firebrick was discarded and replaced. A thin cylindrical rod was used to push on the backside of the coupon to remove from firebrick.

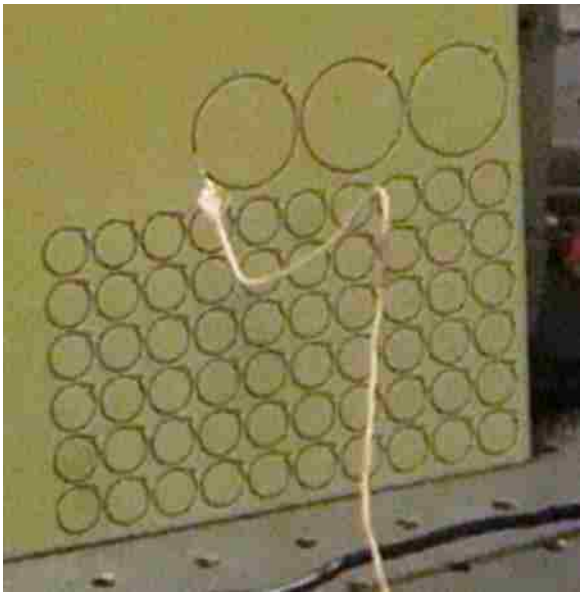

**Figure 3-2: Aluminum Coupons 1cm in Diameter After Cutting with a Water Jet**

### 3.3 Xenon Flash Lamp

The xenon flash lamp's original configuration produced a collimated light to produce near uniform intensity across a square section or space. Manufacturer's configuration had the xenon flash lamp pointed down towards table, as shown in Figure 3-4. This configuration did not physically allow for further focusing of the beam. The xenon flash lamp had to be turned on its side (no new braces or supports were required to do this) and the rail to attach stands was placed underneath the lens and aligned with the axis of the lens where the light is emitted.

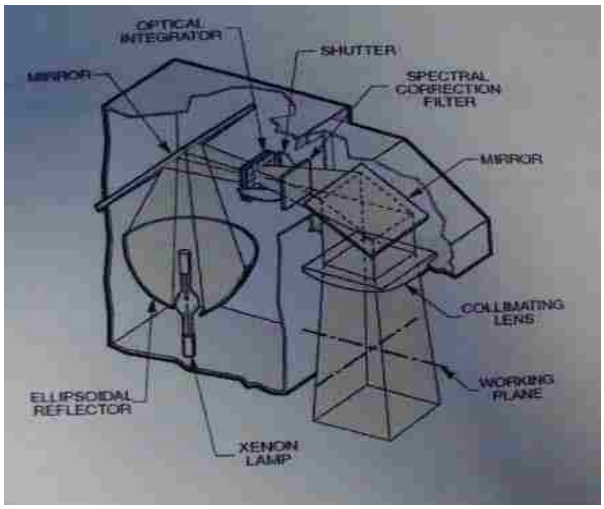


**Figure 3-3: Schematic of how Xenon Flash Lamp Light is Emitted.**

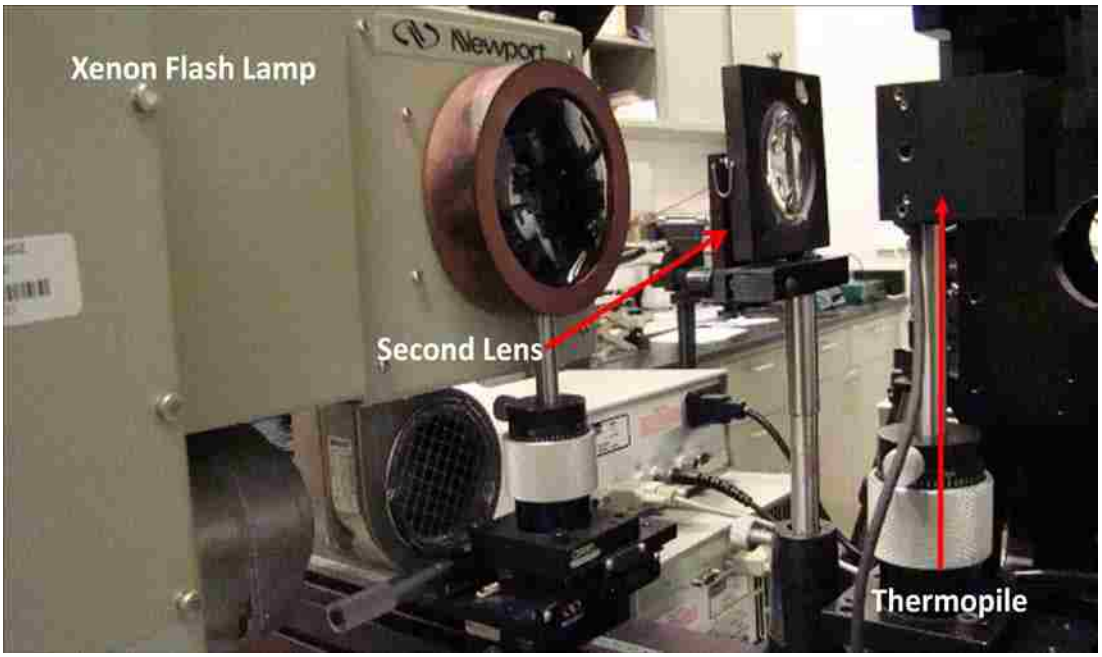


**Figure 3-4: Energy Measurement Configuration**

The xenon flash lamp was connected to a power supply set to a specified value (800W, 1000W, 1200W and 1600W) to ensure thermal loading is constant. The intensity was measured by exposing the Newport Thermopile to the beam depicted in Figure 3-4. Spot size of the focused xenon beam was confirmed using the FLIR thermal camera viewing the front firebrick and coupon shown in Figure 3-5. The left side of Figure 3-5 shows a higher temperature due to previous smoke deposited from burning coupons on the firebrick turning it black leading to increased absorption. Coupons show an oval shape in the frames from the thermal camera in the front because the camera had an angular offset. This had negligible effects on the data collected however the data generated had to be cropped and removed from the data set so that only data from the coupon was considered. The data from the thermal camera in the back also shows as an oval shape because of the square display the rectangular 120x640 pixel region, and the techniques required to crop data for the coupons only described later in this section were also rectangular regions displayed in a square frame.

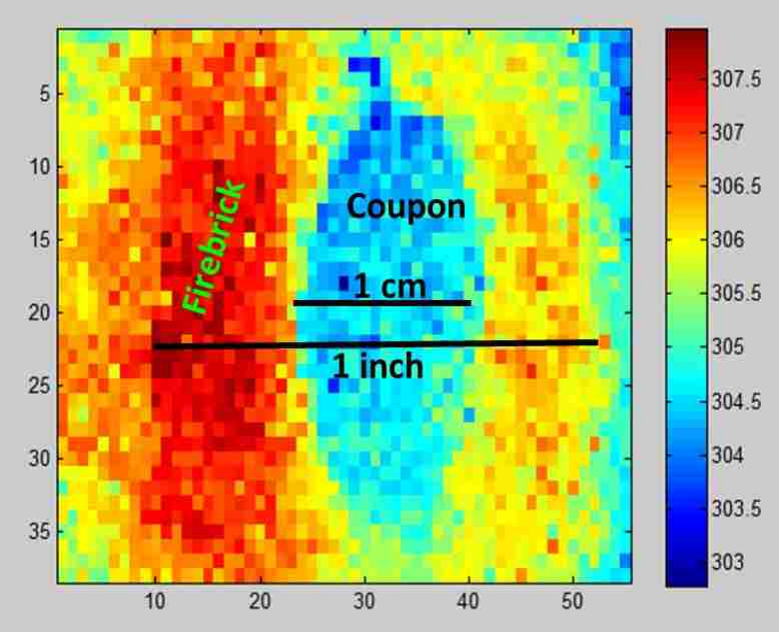


**Figure 3-5: The thermal camera in the front Image of Laser Initiation showing Laser is 1 Inch in Diameter and Firebrick is not Conducting Heat to or from Coupon**

A Compaq desktop computer controlled the xenon flash lamp power and shutter using a MatLab command script. The MatLab script displayed warnings and asked for yes and no inputs to ensure safety goggles are on before opening the shutter. The xenon flash lamp remained on until smoke was released from the coupon. Smoke signifies the onset of color change due to thermal degradation of the epoxy-polyamide primer. Small amounts of smoke were hard to detect while protective eyeglasses or goggles were worn. Therefore, the use of an unfiltered video recording was required to detect smoke.

### 3.4 Data Collection

Two FLIR cameras were used to measure the temperatures of the front and back surface of the coupon. The frame rates of the two thermal cameras were not able to match frame rate because of the programming of the thermal cameras. The 2:1 ratio of frame rates in favor of the thermal camera in the front were chosen. The frame rate was set to 50 frames per second for the SC660 FLIR thermal camera, viewing the front surface or the epoxy polyamide primer. However, this was slightly above what the computer could process and the actual frame rate varied (about 45 fps were recorded). The FLIR SC665 viewing the back of the coupon was set to record at a frame rate of 25 frames per second. Knowledge of epoxy resins and compounds used for fire protection and insulation purposes (11) determined that the back surface would have a slower rate of temperature increase. The orientation of the thermal camera in the back to the coupons can be seen in Figure 3-6.

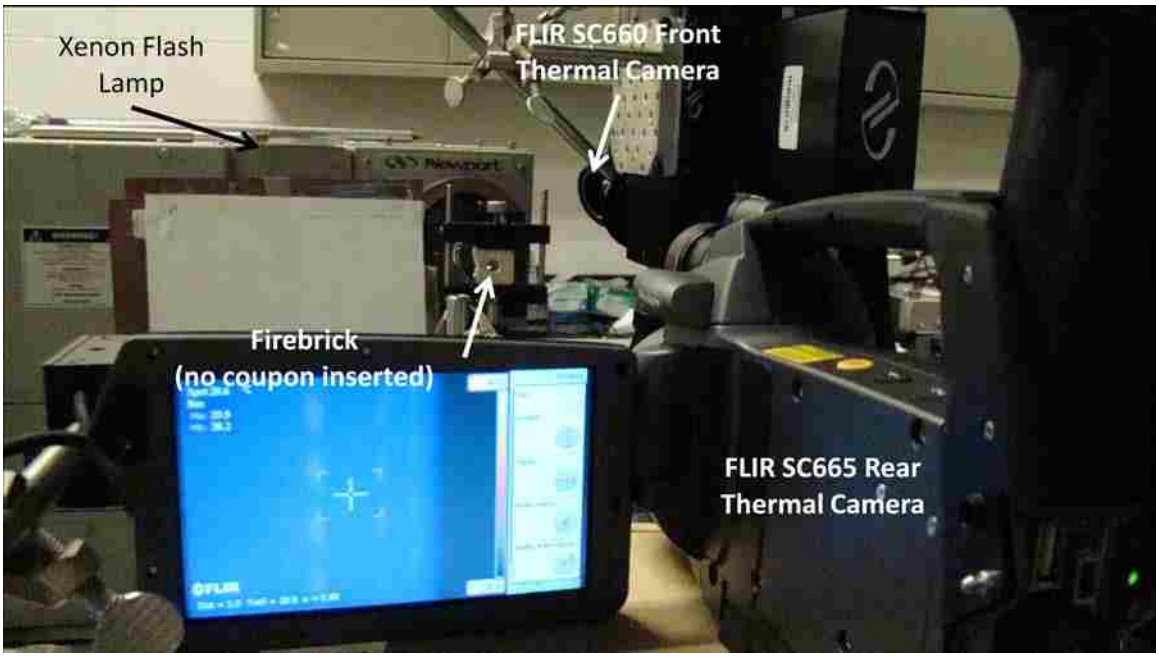


**Figure 3-6: Rear View of Experimental Setup Showing the Thermal Camera in the Back Orthogonal to Firebrick and Coupon**

The data was transferred from the thermal cameras to the Dell laptop and HP desktop and then exported as comma separated values (.csv) or tagged image file format (.tif). The .tif format was used after the discovery that MatLab could accept the format and the export and import of data was therefore more efficient (.csv format took 30~40 minutes from camera to external hard drive and took about 2Gigabytes per coupon test, .tif format took 20~25minutes from camera to external hard drive and took about 1.6Gigabytes per coupon test). The data was then moved to an external hard drive for ease of data retrieval and post processing.

The video capture from the Sony camera recorded at a set rate of 30 fps. Video was recorded in 320p standard definition video. A frame rate of 30 fps had enough fidelity to observe the formation of smoke from the epoxy polyamide. The Sony camera had a built-in auto focus and aperture setting causing initial frames

of the flash to be saturated. The camera adjusts the aperture to reduce the amount of light it receives to observe smoke from coupon. These videos were saved to an external hard drive and were used to determine when degradation began. Windows Moviemaker was used to determine the frame that the smoke first appeared on the epoxy polyamide surface of the coupon.

A Newport Thermopile was used for measuring the intensity of the focused xenon flash lamp beam. An iris was used to reduce the spot size of the beam to accurately measure the intensity of energy to which the coupon was exposed. The area of the Iris is input for the Newport control box to calculate the incoming flux in units of $\frac{W}{cm^2}$ .The measurement required the Thermopile to be mated to the iris, or the beams spot size would be too large for the Thermopile measurement due to light diffusion. Measurement information was displayed on the Thermopile control box, shown in Figure 3-7, and recorded in a notebook.

**Figure 3-7: Newport Thermopile Control Box, Display Energy in W/cm$^2$ for different bulb power settings**

### 3.5 Setup and Procedure

Due to the small size of the coupons, all the cameras and flash lamp were confined to a small area making setup difficult. The video camera was moved to the side of the sample; the thermal camera in the front was located on the opposite side of the coupons and xenon flash lamp but further back towards the lamp as shown in Figure 3-8. Figure 3-8, shows the beam diameter over the

coupon without the firebrick, the focus of the lens is behind the coupon to obtain the 1-inch diameter spot size. The firebrick absorbed or reflected the remaining beam that was not incident on the coupon. The firebrick blocking the remainder of the beam was required to ensure the thermal camera in the back did not record the incident beam in the temperature measurements. The xenon flash lamp lenses and coupon axes were all coincident with each other to ensure maximum beam energy was centered on the coupon. A thermopile replaced the coupon to measure the intensity power of the xenon flash lamp.

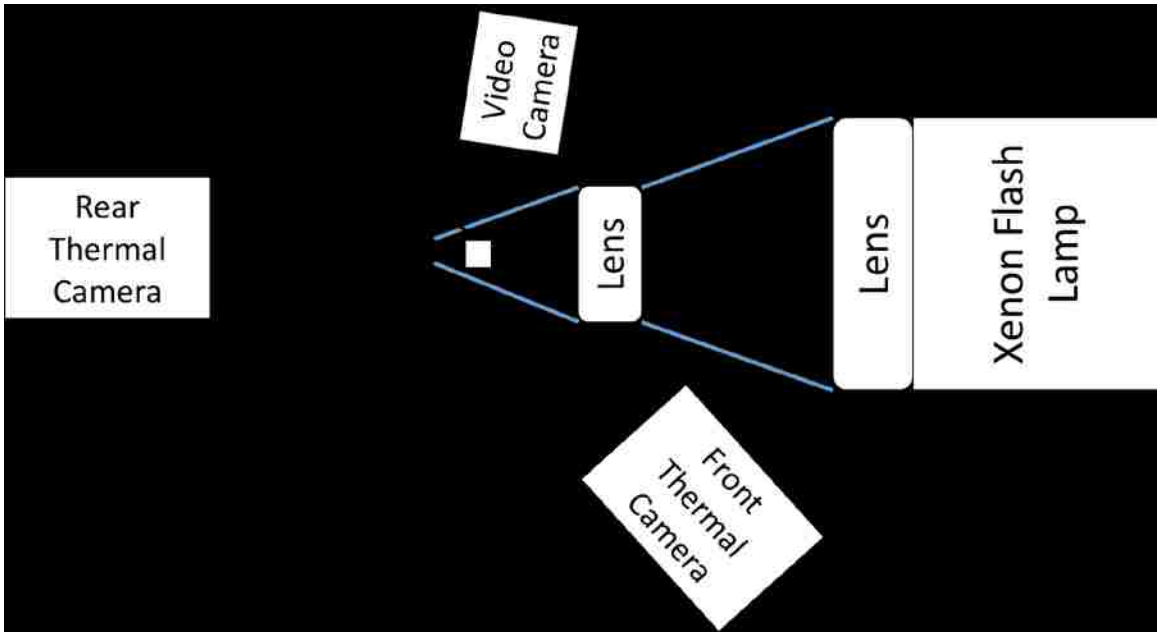


**Figure 3-8: Schematic Top View of Cameras, Coupon, Beam and Xenon Flash Lamp Locations**

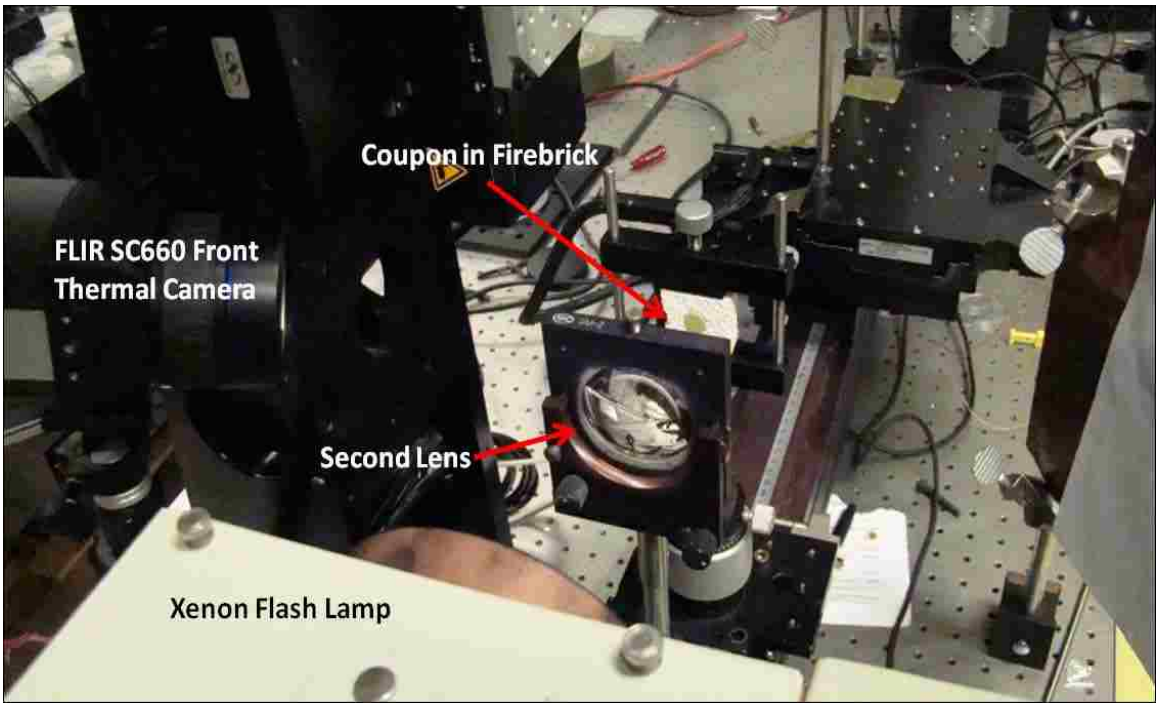


**Figure 3-9 Setup of Experiment in Nearly Ready Configuration.**

FLIR cameras were set to record the frames in the ExaminIR software on both computers connected to the FLIR cameras. Sony camera started recording before the shutter opens. The coupon was flashed until smoke was visible. The Compaq computer closed the shutter and turned off the xenon flash lamp, when the enter key was pushed. The Sony camera and the two FLIR cameras stopped recording data about 30 seconds after the flash was stopped. The coupon was allowed to cool before removing, to avoid melting gloves and burning hands. The cooling time of the coupons and firebrick ensured firebrick did not become so hot that it began conducting heat into future coupons.

### 3.6 Limitations

Several limitations existed that were not solved when performing these experiments. One of the biggest improvements that could be made is by connecting all measurement equipment to a single controlling computer. The

current configuration required four user input devices and time synchronizing between the devices was not possible. The four devices (two desktop computers, laptop computer, and video camera) were not connected to a single network due to current lab setup and available equipment. The lab needs to be updated to have a computer containing higher amounts of ram, processing speed, useable communication ports (adapters are necessary to use USB for all communication), than the computers currently available in the lab. A single point of control is difficult to set up properly because of space and computer limitations. The thermal imaging program may need to be open in two different windows on the same machine to record the two different thermal videos because the ExaminIR software only connects to one FLIR thermal camera at a time. Running experiments from a single computer would synchronize xenon flash lamp shutter opening, temperature data, and a sensor to measure reflectivity of the epoxy polyamide coated aluminum coupons.

**Figure 3-10: The Laptop computer exporting recorded data to portable hard drive**

Visual damage inspection was not very accurate, but was the only available method to receive information in a scientific way on the actual time from xenon flash lamp incidence to the initiation of degradation. The smoke could

have been released from the epoxy polyamide and not visible from the side of the firebrick and coupon, the camera was placed. The coupon's reflectance changed during thermal loading, and a sensor to detect when this happened (to determine when the degradation occurred) is more accurate than visual inspection of video stills. The coupons reflectance itself is a limitation, which caused the camera to make major aperture adjustments to be able to record while the high intensity light was focus on the coupon. Under normal lighting of the Lab, the camera had a larger aperture, which, allowed too much of the xenon light into the camera. The camera lenses auto-focus had to adjust the aperture to reduce the amount of light incoming to the sensor. Eye protection limited ability to observe smoke in order to turn off the Xenon flash lamp at the first instant of smoke.

# 4 Post processing Techniques

Data collected from the experiment was not immediately useable and needed to be filtered and cut. The video recording needed the least amount of editing, but there was a need to process data in the video recording to identify the duration of the flash. The review of the video recordings needed a time display for each frame to calculate the duration of flash until smoke became visible. The thermal data required digital image analysis software that was able to remove many of the recorded pixels that are not from the coupons' surfaces as shown in Figure 4-1, Figure 4-2 and Figure 4-3. The image processing required for the thermal camera recordings needed to calculate the statistics of the temperature profiles for each frame over the coupons' surfaces. Image processing required calculations to determine the frame at which smoke occurred, and plot the mean temperatures of coupons' surfaces to determine when the flash from the xenon flash lamp started and ended.

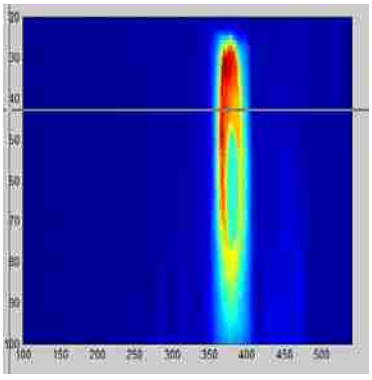

**Figure 4-1: Initial Crop of Front Thermal Image**

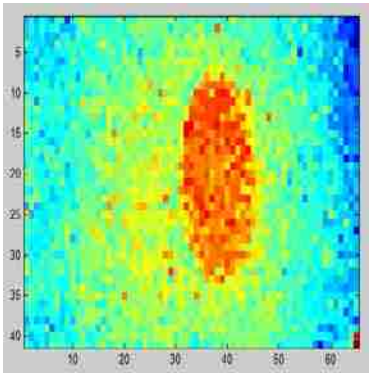

**Figure 4-2: Front Image Zoomed to Area Around the Coupon**

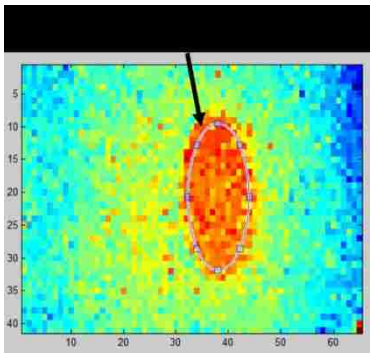

**Figure 4-3: Coupon Selected from The thermal camera in the front Image**

## 4.1 Video Results

Video is recorded using the Sony Camera is used to determine the actual time until smoking occurred. The video time is accurate to a 1/30 of a second based on the standard video frame rate of 30 fps. Windows Movie Maker is a free suitable software that allowed videos to be clipped at both ends to reduce memory required to store videos. Window Movie Maker allowed the viewing of videos frame by frame. Smoke initiation times were determined by the first frame where smoke appeared on the surface of the coupons. This data was recorded in a Microsoft Excel spreadsheet. The times found from the video recordings were saved as a .csv file format for use in MatLab to synchronize the thermal image frame of when burn initiation occurs. The times found using Windows Movie Maker were used to calculate the energy. The measured power recorded from the Newport Thermopile for the power settings of the xenon flash lamp, shown in Table **4-1**, were multiplied by the time of exposure for each coupon. A select sample of data and energy calculations is provided in Table 4-2. Energy was calculated by the equation $E = Pt$ where P is the incident power and t is the exposure time until smoke became visible.

**Table** 4-1**: Relation Between Xenon Flash Lamp Power Setting and Incident Energy on Coupon**

| Bulb Wattage [W] | 800 | 1000 | 1200 | 1600 |
|---|---|---|---|---|
| Incident Energy $\left[\frac{W}{cm^2}\right]$ | 14 | 18 | 23 | 31 |

**Table 4-2: Select Data Sample of Energy Calculations**

| Coupon# | Lamp On [s] | First Smoke [s] | Lamp Off [s] | Duration to Smoke [s] | Lamp Duration [s] | Bulb Power [W] | Energy deposited [J/cm$^2$] | AL type |
|---|---|---|---|---|---|---|---|---|
| 2 | 0.13 | 16.00 | 16.69 | 15.87 | 16.56 | 800 | 228.5 | 2024-T4 |
| 27 | 2.17 | 17.31 | 20.89 | 15.14 | 18.72 | 800 | 218.0 | 2024-T4 |
| 49 | 3.63 | 9.27 | 10.01 | 5.64 | 6.38 | 1200 | 129.2 | 2024-T4 |
| 62 | 4.33 | 18.63 | 20.77 | 14.30 | 16.44 | 800 | 205.9 | 7075-T3 |
| 86 | 3.26 | 16.81 | 19.45 | 13.55 | 16.19 | 800 | 195.1 | 7075-T3 |
| 107 | 2.28 | 17.29 | 18.97 | 15.01 | 16.69 | 800 | 216.1 | 7075-T3 |
| 118 | 1.46 | 10.10 | 12.87 | 8.64 | 11.41 | 1600 | 268.1 | 7075-T3 |
| 135 | 2.90 | 12.14 | 13.35 | 9.24 | 10.45 | 1200 | 211.6 | 2024-T4 |
| 147 | 2.55 | 11.88 | 14.04 | 9.33 | 11.49 | 1000 | 170.7 | 2024-T4 |

## 4.2 Thermal Camera Data Export

The data export formats available from the ExaminIR software (used to record thermal image recordings from the FLIR thermal cameras) were initially individual frames exported as a Comma Separated Value (.csv) format. The large number of files used too much memory. Each frame in .csv format was greater than 1Mbyte, and each coupon exposed for many seconds caused the number of frames for each coupon's data to number in the thousands. The file generated by the ExaminIR program was also around 1Gbyte in size for each coupon's exposure recording (for each back and front recording). This gave a total of about

3~4Gbytes of memory per coupon. This put computers at risk of becoming unstable during the future coupon exposures. Frame skipping was used for data from the rear SC665 Thermal camera to reduce the memory size, but this was determined to be an unacceptable export as the skipping function did not skip at the specified intervals. The Tagged Image File Format (.tif) was used once it had been determined that the MatLab image processing software was able to read the “stacked” images in this format as a single variable. Each frame was recorded along the depth dimension and in order to allow a single file of about 750Mbytes to be exported this made the total memory taken by each data set for the coupon to be around 2Gbytes vs. the 3~4 use by the .csv format.

### 4.3 Image Processing

MatLab was used for the image processing. It can read images where a single number at each pixel is used to scale the image, and not three RBG values. The scaled image has enough contrast between the firebrick and the coupon in frames to be able to identify where the coupon is in relation to the recorded pixels. This region can be selected using an elliptical mask created in MatLab to ignore data for recorded pixels not focused on the coupon in order to generate temperature profiles for each coupon. The images had the same pixel data for a single coupon. However, during coupon removal or other people present in the lab the thermal cameras may be knocked or moved, thus requiring a new mask and pixels to generate the temperature profiles. To create this mask the overall image is cropped, as seen in Figure 4-4, to allow the user to define a region to zoom into reducing the required memory (see Figure 4-5).

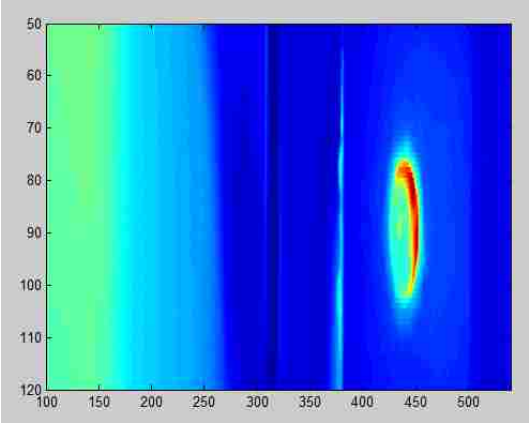


**Figure 4-4: Initial Crop of the Image from the Thermal Camera in the Back**

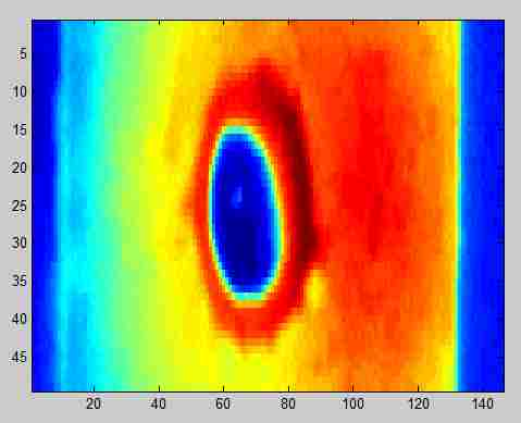


**Figure 4-5: Second Crop of the Thermal Camera Image to Zoom in on the Coupon and Firebrick**

Caution should be used when selecting the zoom area for the region around the coupon (see Figure 4-4). If the region selected (Figure 4-5) is too small around the coupon, the elliptical selection, shown in Figure 4-6, becomes harder to make due to the lost contrast in the scaled image between the firebrick and the coupon. Elliptical mask is selected from thermal camera data with pixels zoomed large enough to select the coupon, without gathering data for the firebrick. Cropping the image is especially important for the .tif stacked images, as several variables contained all of these stacked images. The .csv images are opened one at a time and the random access memory limitations are less of a concern.

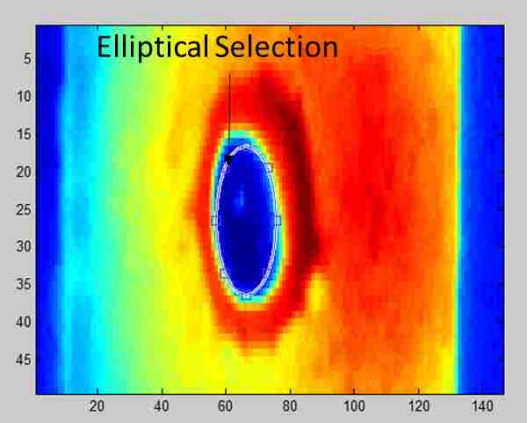


**Figure 4-6: Ellipse used to Select Data for the Coupon from of Image from the Back**

## 4.4 Synchronizing Video and Thermal Data

All the previous steps in the post processing of the data have given the temperature profile for the entire thermal camera recording, the times to the first visible smoke, the total flash time of the Xenon Flash Lamp, and the location of the coupon with respect to the pixels recorded for the flash heating experiment. The video frames need to be linked to the thermal camera frames so the temperature and video data are synchronized. To do this the flash is defined by an increase in temperature on the front surface as seen in Figure 4-7.

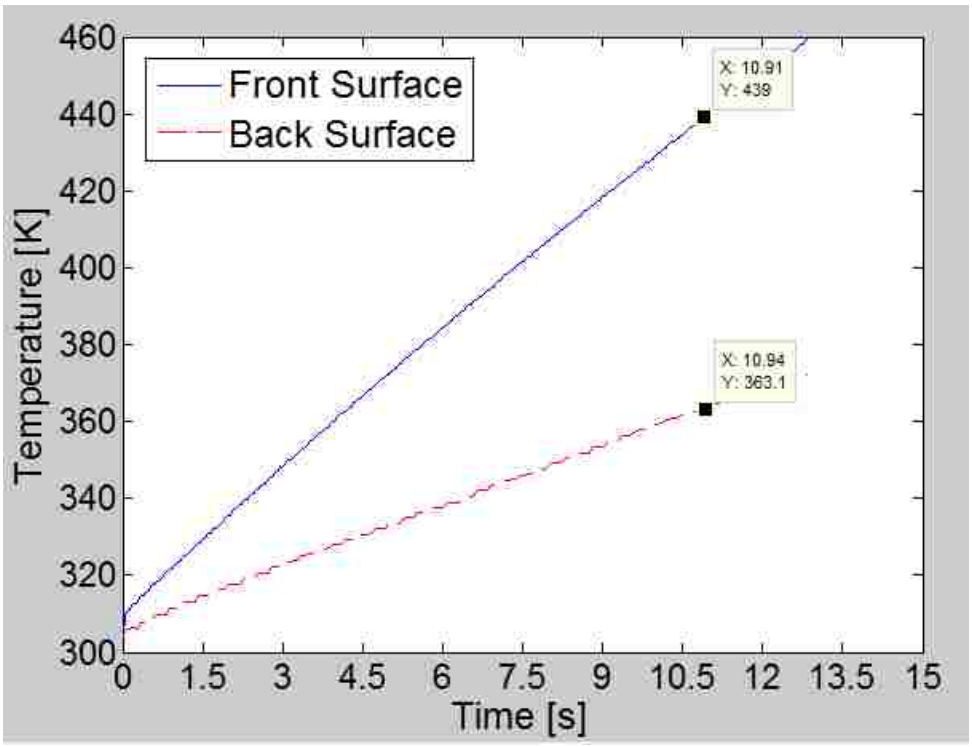


**Figure 4-7: Temperature Profile of Epoxy Polyamide Primer Surface and 2024-T4 Aluminum Substrate Surface. Incident Power 18$\frac{W}{cm^2}$, time to degradation 10.9s and 12.8s total exposure.**

The thermal camera in the back recorded a lower temperature on the back surface as expected. This result is expected because the front surface is supplying the heat to the rear of the coupon through conduction. The front surface remained warmer because of the lag in response of the rear surface and the lower conductivity of the epoxy polyamide. It is harder to measure the flash start time and the flash end time because the temperature slightly lags in time behind the front surface. This lag is due to the stored energy in the epoxy and aluminum substrate continuing to heat the back surface even after the flash has finished. A temperature time history with respect to the recorded frame for the rear aluminum substrate is shown Figure 4-7. The number of time data point are doubled for the front surface because of the different frame rates of the thermal

cameras. The frame rate was 50 frames per second for the camera recording the front surface and 25 frames per second for the thermal camera recording the back surface. The start and finish points labeled in the figures show a reduced temperature increase with time, because the transfer of heat to the substrates back surface (nearly linear rise to a lower temperature on the back surface in the same amount of time).

# 5 Results

## 5.1 Temperature Data

Temperature distribution for the coupon during thermal loading applied by the Xenon flash lamp is necessary. This was because the statistics for the mean temperatures of the coupon sample size were calculated using the average temperature over the surface of each coupon at the time of burn initiation. Figure 5-1 shows the standard deviation at the frame of burn initiation. The deviations of temperature across the coupons were low enough to use a mean value for the temperature as a reasonable representation of coupon temperature. Higher deviations of the coupons surface temperature were recorded in other frames. These higher deviations of coupon surface temperature are due to the thermal camera performing a Non-Uniformity Calibration (NUC) of the thermal recording. Some of these occurred during the time the xenon flash lamp was in operation, but all NUCs were automatically performed by thermal cameras after the shutter of the xenon flash lamp closed. The mean burn initiation temperatures are shown in Figure 5-2 for all coupons. There does seem to be some grouping of burn initiation temperature data with respect to the incident flux. Statistical analysis was performed to determine whether the burn initiation temperature increases with flux, as in other un-mounted epoxy resin studies (9) (15) (2) (11), or if temperature data gathered shows a single burn initiation temperature.

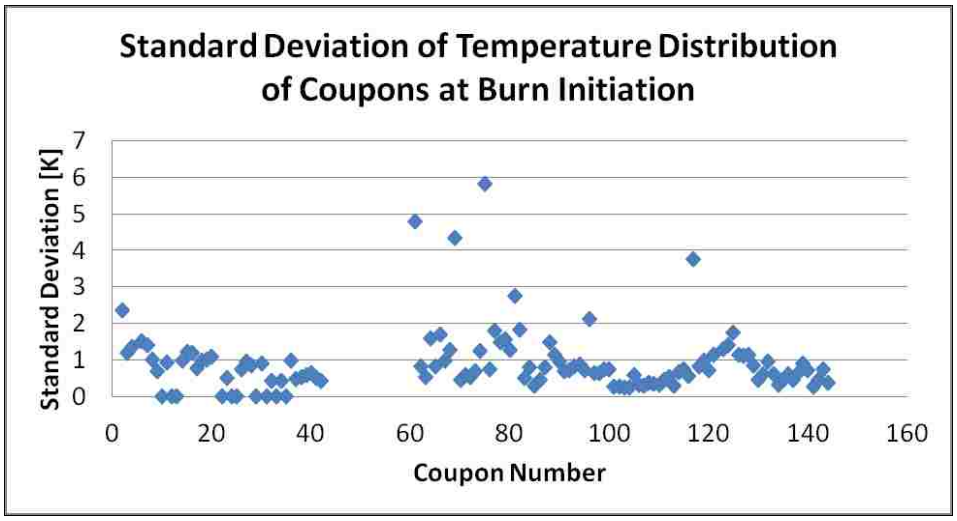


**Figure 5-1: Standard Deviation of All Pixels on Coupon Surface at Frame of Burn Initiation**

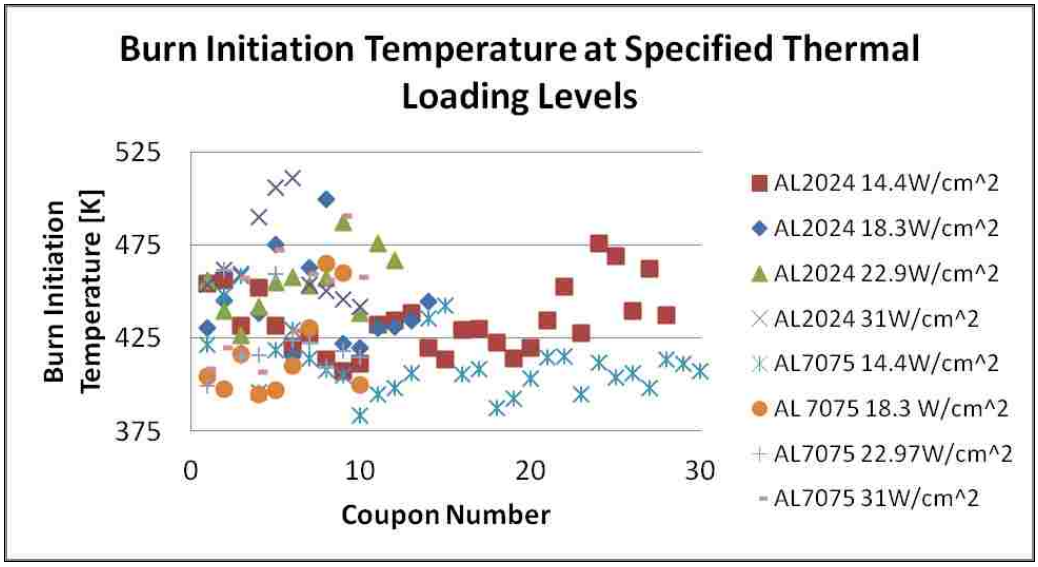


**Figure 5-2: Mean Temperature of Burn Initiation Grouped by Incident Thermal Flux and Aluminum Substrate Type**

The time to initial burn was detected with the Video Camera recording using Windows Movie Maker to find the frame and the corresponding time when smoke appeared. The temperature of epoxy polyamide degradation was recorded by the front SC660 FLIR thermal camera using the time from the video camera. The uncertainty associated with this type of measurement is about $\frac{1}{30}$ s of when burn

initiation occurs, due to the Video recording frame rate of 30 frames per second that was set by the Sony camera. Frame rate for the thermal camera in the front was faster at about 45 frames per second. Once the burn initiation temperature was found for the 123 coupons that had complete thermal data, the statistics were calculated in Table 5-1. The burn initiation statistics for the epoxy polyamide are shown in Table 5-1. The statistics were calculated assuming a normal distribution of the population. Coupons sampled mean degradation temperature is $\overline{y} = \frac{\sum_{i=1}^{n} y_i}{n} = \mu$. Here $y_i$ is the value of the degradation temperature of a single coupon, n is total number of coupons under the specified thermal loading. The sample standard deviation is $S = \sqrt{\frac{\sum_{i=1}^{n}(y_i - \overline{y})^2}{n-1}}$ (16).

**Table 5-1: Burn Initiation Statistics of Epoxy-Polyamide on Aluminum 2024-T4 and 7075-T3 substrates**

| AL Type | Incident Power (W) | Mean Temp. [K] | STD Dev. [K] | STD Error [K] | T-factor | Mean Min [K] | Mean Max [K] | Margin of Error [K] |
|---|---|---|---|---|---|---|---|---|
| 2024-T4 | 14.4 | 434.2 | 18 | 0.67 | 1.7 | 433.1 | 435.4 | ± 1.14 |
| 2024-T4 | 18.33 | 440.5 | 24.07 | 1.85 | 1.76 | 437.3 | 443.8 | ± 3.26 |
| 2024-T4 | 22.97 | 454.5 | 17.96 | 1.63 | 1.78 | 451.7 | 457.5 | ± 2.91 |
| 2024-T4 | 31.03 | 467.3 | 25.39 | 2.82 | 1.81 | 462.3 | 472.5 | ± 5.11 |
| 7075-T3 | 14.4 | 411.2 | 17.35 | 0.6 | 1.7 | 410.3 | 412.3 | ± 1.02 |
| 7075-T3 | 18.33 | 417.6 | 26.13 | 2.9 | 1.81 | 412.4 | 423.0 | ± 5.26 |
| 7075-T3 | 22.97 | 423.9 | 20.48 | 2.28 | 1.81 | 419.8 | 428.1 | ± 4.12 |
| 7075-T3 | 31.03 | 445.7 | 28.28 | 3.14 | 1.81 | 440.1 | 451.5 | ± 5.69 |

Prior to experimental research, the burn temperature was anticipated to be similar regardless of the incident flux. This is because the flux was faster than previous research conducted at the rate of temperature increase of 5°C/min. Thermal loading for the lowest incident wattage (14.4$\frac{W}{cm^2}$) has an effective heating rate of 500 °C/min. Temperature measurements show a trend as the flux increases so does the burn initiation temperature. However, there are some overlapping bounds of the burn initiation temperatures for the primer coated aluminum substrates. The lowest power setting for both substrates had the most samples, and the standard deviations for them were small, while the higher energy settings had the fewer samples and had larger standard deviations. The results are plotted in Figure 5-3 where the cases refer to the corresponding fluxes as shown in Table 5-2. From these plotted mean and error bounds it can be seen that there is significant overlap in the exposed samples. The general trend is still upwards, but more samples are required in order to reduce the standard deviations of the experiment. There appears to be a relation between burning initiation and flux. Statistical comparison can determine if there is a dependence between burning initiation and flux.

**Table 5-2: Incident Thermal Power Case Number Look Up**

| Incident Power $\left[\frac{W}{cm^2}\right]$ | 14 | 18 | 23 | 31 |
|---|---|---|---|---|
| Case | 1 | 2 | 3 | 4 |

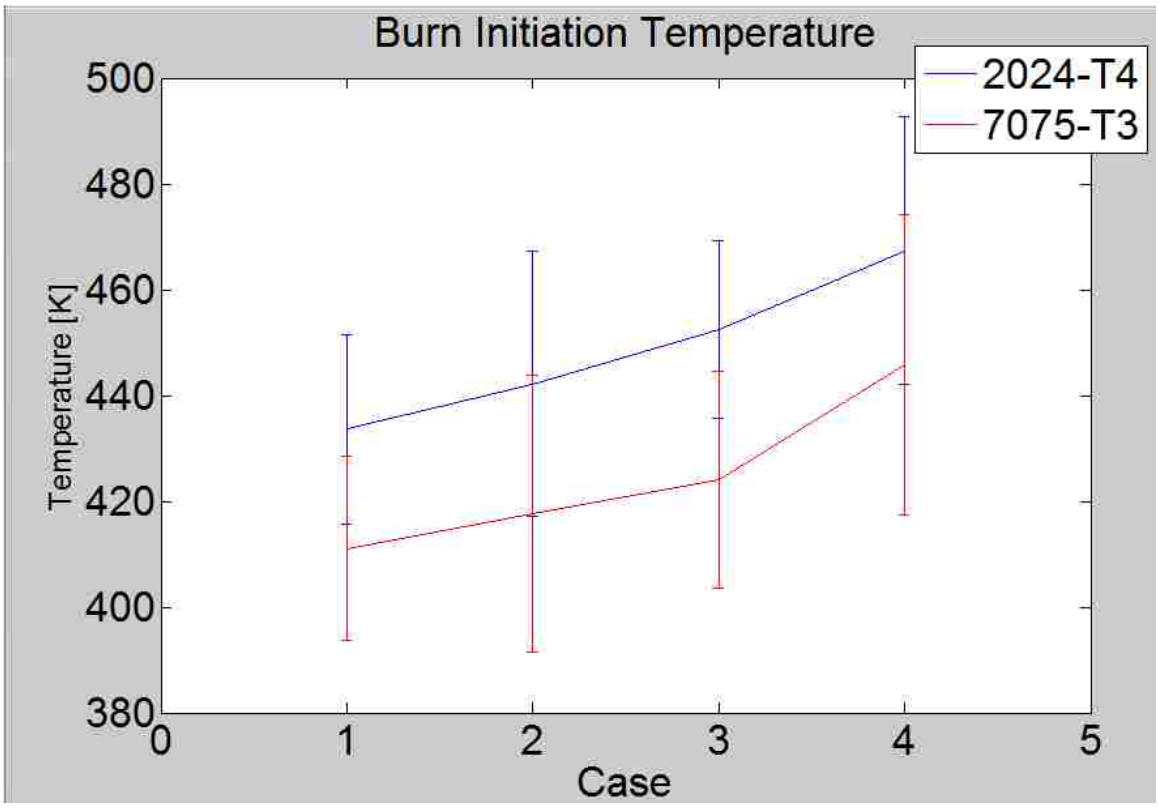


**Figure 5-3: Burn Initiation temperatures Plotted with Error Bounds for Epoxy Polyamide Primer coated Aluminum 7075-T3**

When comparing two sets of data for two different variables of the experiment a Two Sample t-Test can be used to show that, the rise in temperature is either increasing with increasing thermal flux or the mean values of burn initiation are within in the error bounds. This is shown using a statistical hypothesis with two conditions. $H_1, \mu_1 = \mu_2$ and $H_2, \mu_1 \neq \mu_2$. The samples sizes were different and the calculated t statistic used to compare the two samples is:

$$t = \frac{\overline{y_1} - \overline{y_2}}{\sqrt{\frac{S_1}{n_1} + \frac{S_2}{n_2}}},$$

where t is the test statistic. The test statistic is compared to the t-score from the t-distribution from a modified degrees of freedom. The test statistic and the t-score were compared to determine if there was a statistically equal mean within

the given confidence interval. $S_1$ and $S_2$ are the sample standard deviations. The t-distribution degrees of freedom used to look up the t-score that the t statistic from above is compared to, is approximated by:

$$v = \frac{\left(\frac{S_1^2}{n_1}+\frac{S_2^2}{n_2}\right)^2}{\frac{\frac{S_1^2}{n_1}}{n_1-1}+\frac{\frac{S_2^2}{n_2}}{n_2-1}}.$$

This approximation determined the t-score from the t-distribution to compare to $t$. This determined which statistical hypothesis was true (16). A confidence level of 90% was chosen for these calculations and the respective t-values are gathered from tabulated data (16). The hypothesis is tested by comparing the value of t and the tabulated value for $t_{\frac{\alpha}{2},v}$. $H_1$ is true if $|t_0| < |t_{\frac{\alpha}{2},v}|$, which determines if the mean of the data from the two different heating rates, shows a potentially equal mean burn initiation temperature. $\alpha$ is the level of significance or $1 - Confidence\ Level$ for the statistical analyses performed. If $H_2$ is true ($|t_0| > |t_{\frac{\alpha}{a},v}|$), the mean burn initiation temperatures of the two incident flux rates is not equal. Results of the calculations are displayed in Table 5-3 and the results show that the burn initiation temperature is increasing with flux. The Epoxy primer coated Aluminum 2024-T4 shows the mean of burn initiation temperatures for the experiments conducted with 18.3$\frac{W}{cm^2}$ and 22.9 $\frac{W}{cm^2}$ incident thermal flux rates are not statistically different from each other. Using a confidence level of 80% the mean between these two points is increasing with increasing thermal flux. The mean burn initiation temperature for the 22.9 $\frac{W}{cm^2}$ incident thermal flux from the

Xenon flash lamp is greater than the burn initiation temperature for the 18.3$\frac{W}{cm^2}$ incident thermal flux, because the mean burn initiation temperature for 22.9 $\frac{W}{cm^2}$ is greater than the mean burn initiation temperature for 14.4 $\frac{W}{cm^2}$ incident thermal flux rate. Using this statistical comparison the mean temperature of burn initiation for 18.3$\frac{W}{cm^2}$ incident thermal flux rate is potentially the same as the mean temperature of burn initiation for 14.4$\frac{W}{cm^2}$ incident thermal flux rate. This leads to the conclusion that even though between these the samples mean temperature of burn initiation for 14.4$\frac{W}{cm^2}$ incident thermal flux rate are hypothetically equal to the mean temperature of burn initiation for 18.3$\frac{W}{cm^2}$ incident thermal flux rate; the mean temperature of burn initiation for 18.3$\frac{W}{cm^2}$ incident thermal flux rate is hypothetically equal to the mean temperature of burn initiation for 22.9$\frac{W}{cm^2}$ incident thermal flux rate; the burn initiation temperature increases with flux because the mean temperature of burn initiation for 14.4$\frac{W}{cm^2}$ incident thermal flux rate is less than the mean temperature of burn initiation for 22.9$\frac{W}{cm^2}$ incident thermal flux rate.

**Table 5-3: Burn Initiation Temperature Two Sample t-Test Calculated Values for Al 2024-T4-T4 Comparison and Statistical Hypothesis Results**

| Aluminum 2024-T4 | | | | | | |
|---|---|---|---|---|---|---|
| Samples Compared | 1,2 | 1,3 | 1,4 | 2,3 | 2,4 | 3,4 |
| t | -1.732 | -3.566 | -5.806 | -1.405 | -3.116 | -2.698 |
| v | 20.00 | 22.00 | 12.00 | 22.00 | 19.00 | 15.00 |
| $t_{0.025,v}$ | -2.086 | -2.074 | -2.179 | -2.074 | -2.093 | -2.131 |
| $\mu_1 = \mu_2$ | True | False | False | True | False | False |

This very same Two Sample t-Test is carried out for the Epoxy-Polyamide primer coated Aluminum 7075-T3. The calculations were carried out using a 95% confidence interval using the same statistical hypothesis (Table 5-4). Here the confidence level needs to be around 50% to have all data statistically showing an increase in the mean burn initiation temperature. However, at the 95% confidence level the same situation occurs as before with the same incident thermal loading levels. Where, the samples' mean temperature of burn initiation for 14.4$\frac{W}{cm^2}$ incident thermal flux rate are equal to the mean temperature of burn initiation for 18.3$\frac{W}{cm^2}$ incident thermal flux rate. Mean temperature of burn initiation for 18.3$\frac{W}{cm^2}$ incident thermal flux rate is equal to the mean temperature of burn initiation for 22.9$\frac{W}{cm^2}$ incident thermal flux rate. Mean temperature of burn initiation for 14.4$\frac{W}{cm^2}$ incident thermal flux rate is less than the mean temperature of burn initiation for 22.9$\frac{W}{cm^2}$ incident thermal flux rate. Therefore, the mean burn initiation temperature is increasing with increasing thermal loading flux.

**Table 5-4: Burn Initiation Temperature Two Sample t-Test Calculated Values for AL 7075-T3 Comparison and Statistical Hypothesis Results**

| Aluminum 7075-T3 | | | | | | |
|---|---|---|---|---|---|---|
| Samples Compared | 1,2 | 1,3 | 1,4 | 2,3 | 2,4 | 3,4 |
| t | -1.166 | -2.291 | -6.166 | -0.748 | -3.330 | -3.259 |
| v | 11.00 | 13.00 | 11.00 | 17.00 | 17.00 | 16.00 |
| $t_{0.025,v}$ | -2.201 | -2.16 | -2.201 | -2.11 | -2.11 | -2.12 |
| $\mu_1 = \mu_2$ | True | False | False | True | False | False |

## 5.2 Energy Calculations

The burn initiation temperature is an important variable for further modeling efforts, but the amount of energy absorbed should also be investigated, to determine if the absorbed energy also depends on the flux rate. More data points are available for the time to burn, as the video camera did not have data loss due to a erasing of the hard drives of the Air Force Institute of Technology's computers. Experiment was conducted between two different trips, and the time taken to export was too long for the first time out and experimental results were left on the Air Force Institute of Technology's computer hard drives. The absorption is unknown due to lack of available instrumentation. The energy absorption of the epoxy polyamide, as a fraction of the emitted wavelengths, was similar as the wavelengths emitted did not change for the various powers. However, the intensity of the flash wavelengths increases with the power. Taking an absorption coefficient of 1 or a complete absorption the incident energy required to initiate burning was calculated from $E = Pt$ where E is the energy, P is the intensity over area and t is the time determined from video recording. Statistical Calculations for the energy incident on all coupons is calculated and shown in Table 5-5.

**Table 5-5: Incident Energy Statistics of Epoxy-Polyamide on Aluminum 2024-T4 and 7075-T3 Substrates Obtained at the Time of Burn Initiation**

| AL Type | Incident Power [W/cm$^2$] | Mean Energy [J/cm$^2$] | Standard Deviation [J/cm$^2$] | Standard Error [J/cm$^2$] | T-factor | Margin of Error [J/cm$^2$] | Mean Max [J/cm$^2$] | Mean Min [J/cm$^2$] |
|---|---|---|---|---|---|---|---|---|
| 2024-T4 | 14.4 | 190.6 | 28.73 | 1.37 | 2.05 | ± 2.81 | 187.8 | 193.4 |
| 2024-T4 | 18.33 | 170.3 | 31.32 | 1.47 | 2.10 | ± 3.09 | 167.2 | 173.4 |
| 2024-T4 | 22.97 | 171.6 | 48.64 | 2.26 | 2.10 | ± 4.76 | 166.9 | 176.4 |
| 2024-T4 | 31.03 | 171.4 | 47.23 | 2.15 | 2.09 | ± 4.50 | 166.9 | 175.9 |
| 2024-T4 | All | 177.4 | 39.51 | 4.26 | 2.00 | ± 8.52 | 168.86 | 185.90 |
| 7075-T3 | 14.4 | 201.6 | 51.69 | 2.53 | 2.05 | ± 5.18 | 196.4 | 206.7 |
| 7075-T3 | 18.33 | 204.0 | 53.69 | 2.58 | 2.26 | ± 5.84 | 198.2 | 209.8 |
| 7075-T3 | 22.97 | 200.5 | 20.75 | 0.99 | 2.26 | ± 2.25 | 198.2 | 202.7 |
| 7075-T3 | 31.03 | 241.5 | 53.67 | 2.50 | 2.26 | ± 5.65 | 235.9 | 247.2 |
| 7075-T3 | All | 208.5 | 49.82 | 6.43 | 2.00 | ± 12.86 | 195.59 | 221.32 |

The incident energy shows an interesting result for both primer coated aluminum substrates. The primer coated 2024-T4 Aluminum coupons show a nearly equal incident energy at all heating rates greater than the 14.4 $\left[\frac{W}{cm^2}\right]$. This increase in measured incident energy at the lower thermal loading could be due to the aluminum substrate acting as a heat sink removing energy from the primer film, requiring greater energy absorption to reach the energy required to begin degradation. This increase in energy is investigated, due to the error bounds, between the 14.4$\frac{W}{cm^2}$ minimum bound based on a 95% confidence interval showing that there may not be any increase in mean energy for the lower

thermal incident energy as shown in Table 5-4. These results taken as a whole population are similar enough to determine that the mean lies between 169$\left[\frac{J}{cm^2}\right]$ and 186$\left[\frac{J}{cm^2}\right]$ with a 95% confidence level shown in the 6th row in Table 5-4.

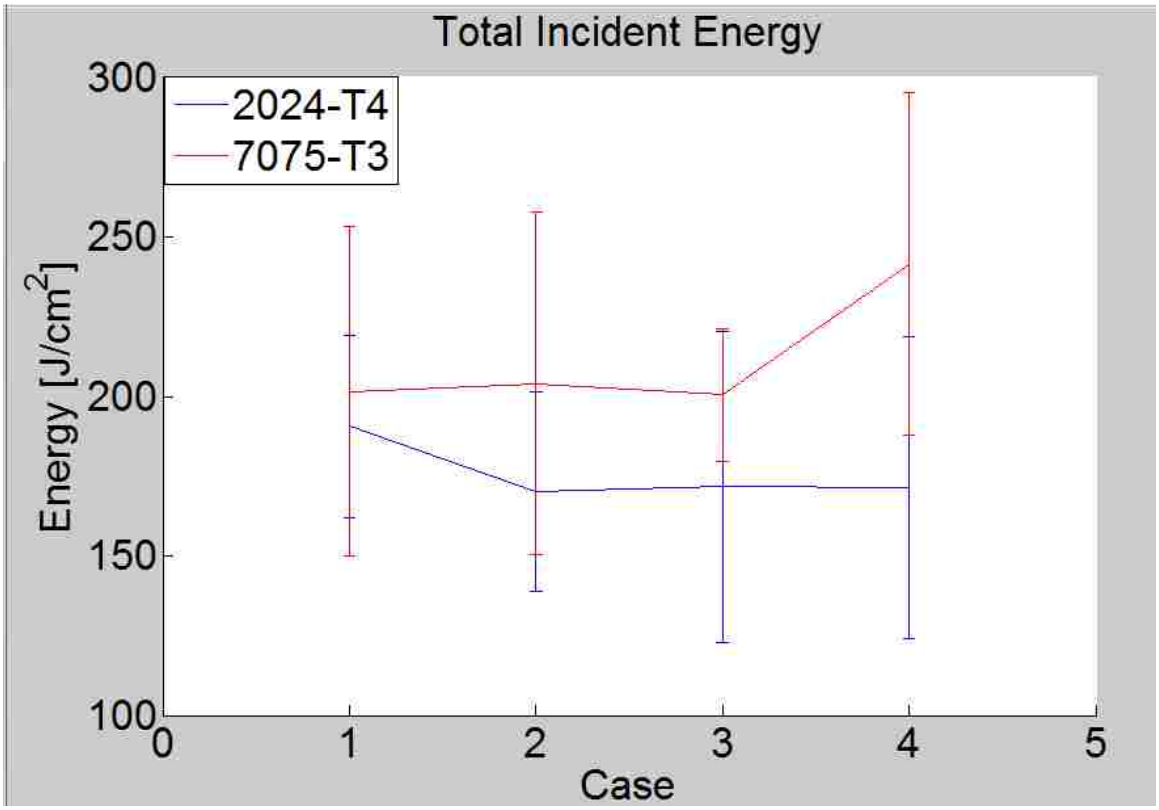


**Figure 5-4: Incident Energy for Initiation of Epoxy-Polyamide Primer Degradation on 2024-T4-T4 Aluminum Substrate with Margin of Error Bounds Included**

The primer coated 7075-T3 Aluminum showed a different trend. These coupons have an overall higher energy required to initiate degradation. The ratio of energy absorbed is 1.175 in favor of the 7075 aluminum substrate coupons. The 7075-T3 aluminum is 1.52 times as thick as the 2024-T4 aluminum, therefore the 7075 is expected to remove more energy from the epoxy polyamide film. Absorbed energy is nearly the same for all incident thermal loading except the highest, 31.03$\left[\frac{\mathrm{W}}{\mathrm{cm}^2}\right]$, incident thermal loading; at this loading level the

absorbed energy seems to increase as shown in Figure 5-4. Using the recorded data for all mean of 7075-T3 aluminum substrates the statistical comparison shows that the variation of data is within the ranges of standard error. Based on a 95% confidence level the mean energy required is between 196$\left[\frac{J}{cm^2}\right]$ and 221$\left[\frac{J}{cm^2}\right]$ shown in the last row of Table 5-5. This increase is due to the thicker substrate absorbing more of the energy deposited on the epoxy primer film.

### 5.3 Model Comparison

The time of exposure for the model was calculated from the total mean energy from the experiment divided by the measured flux. These run times for each aluminum type and power setting are displayed in Table 5-6. Using these run times allowed for the model to accurately predict the front surface temperature of the epoxy. The model uses a Forward Time Center Space finite difference method. This method was chosen due to computer limitations and time to run each case. This FTCS model takes between 1 and 3 minutes, while the Crank Nicholson Galerkin method took up to 20 hours. The Crank Nicholson Galerkin model required a matrix inversion of a very large matrix and had oscillations in the first few time steps that could cause the model to become unbounded. The absorption based on the model was 60%, which seemed reasonable with respect to research conducted for the cool colors project funded by California State (17). The epoxy polyamide was pigmented with green and yellow chromates. The green and yellow chromates have very different reflectance properties. The green chromates typically absorbed 65% of the near infrared light and the yellow absorbed 20% of the near infrared (17). These

absorptions change for the Visible and UV spectrums. The yellow pigments absorb more of the incident energy and the green pigments absorb less of the incident energy. The use of chromate in the epoxy polyamide for the entire spectrum was determined to be between 40% and 70% from the data provided by Levinson et al. The total mean energy absorbed was calculated by multiplying the total mean absorbed energy at burn initiation and the absorption found using the model. The total absorbed modeled energy 106$\frac{J}{cm^2}$ for the 2024-T4 Aluminum coupons and 125$\frac{J}{cm^2}$ for the 7075-T3 Aluminum coupons.

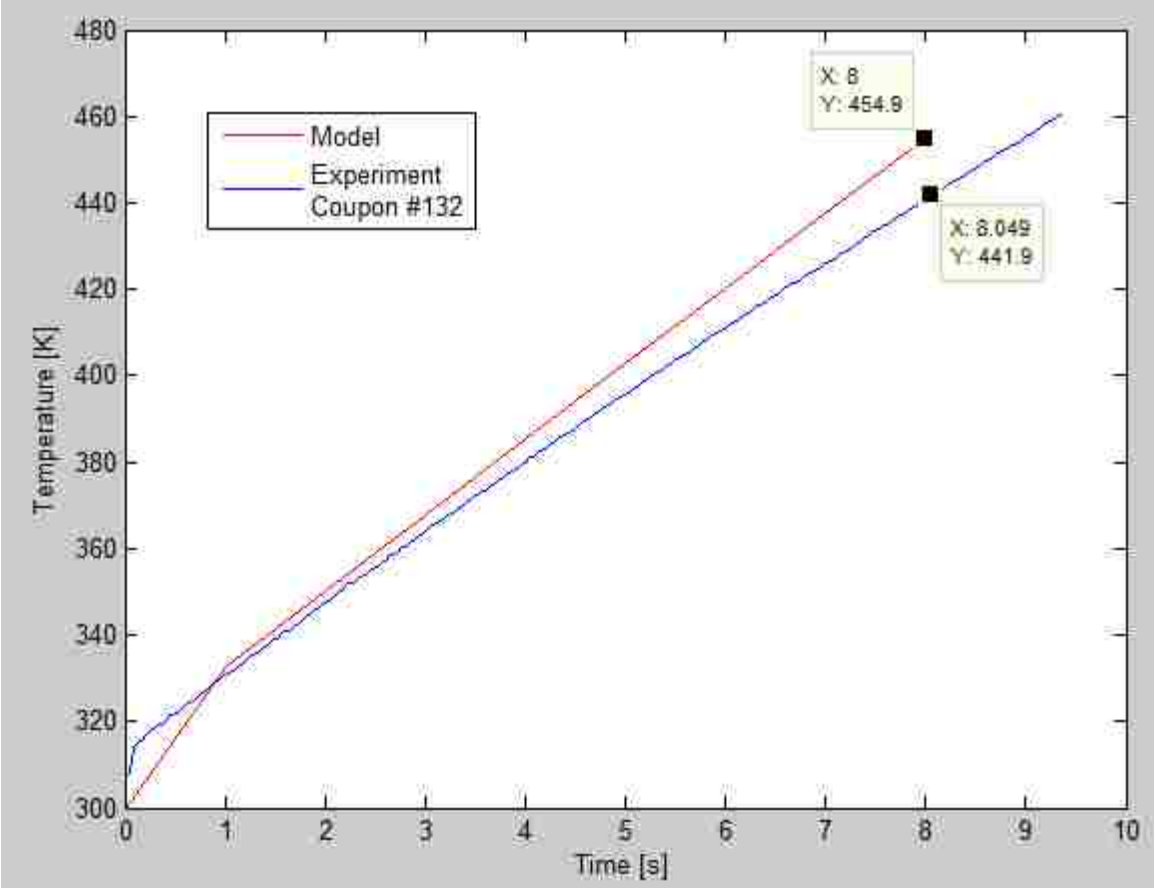


**Figure 5-5 Comparison of the Model and Experimental Measured Temperature Data from the 132nd Coupon Exposed with a 2024-T4 substrate and a 18W/cm$^2$ Exposure for 8 seconds**

Dividing by the area of the coupon surface (0.785cm$^2$) the modeled absorbed energy was 83.6 J and 98.2 J for the burn initiation of the epoxy polyamide primer surfaces are tabulated in Table 5-6. The model compared to a single coupon is shown in Figure 5-5 displaying a 2% variance at the time of burn initiation. The model has about a 1% discrepancy from the measured values, an acceptable fit considering the absorption coefficient changed slightly for the different aluminum substrates. This absorption is visually different for the two substrates as shown in Figure 5-6, and there is a large portion of incident energy in the visible spectrum. This led to the idea of using a slightly higher absorption coefficient for the model for the 7075-T3 aluminum substrate.

**Figure 5-6: Surfaces of 2024-T4 and 7075-T3 Aluminum Substrates**

The absorbed energy in the epoxy polyamide primer based on the model is 0.46 J and 0.35 J for the 2024-T4 and 7075-T3 aluminum substrates. The energy density obtained, based on the 0.0008 inch film thickness used in the model, is 288 $\frac{J}{cm^3}$ for the epoxy polyamide on the 2024-T4 aluminum substrate and 220 $\frac{J}{cm^3}$ for epoxy polyamide on the 7075-T3 aluminum substrate. This shows heating rate dependence on the epoxy polyamide film due to substrates

energy capacity. Pigments and the type of substrate affect the absorption persenctage. These have been shown to have a significant effect on energy absorption in painted surfaces by the State of California (17). The temperature profile at the point of epoxy polyamide degradation is displayed in Figure 5-7. In this figure it is seen that the epoxy polyamide initially heats up to provide the heat to the aluminum substrate, but as the exposure continues the epoxy temperature difference at the surface and the aluminum substrate appears to be fairly constant. The aluminum is not all at the same temperature, but the variation is small due to the high conductivity of the aluminum. The heat flows very quickly to the back surface once though the epoxy polyamide and into the aluminum substrate.

**Table 5-6: Calculated Model Run Times for Temperature Profiles Determined By Mean Energy and Measured Incident Power Data with Modeled Temperature and Calculated Mean Temperature**

| Aluminum Type | Mean Energy Calculated $\left[\frac{J}{cm^2}\right]$ | Incident Power $\left[\frac{W}{cm^2}\right]$ | Calculation Time [s] | Modeled Maximum Temperature [K] | Measured Mean Temperature from Data [K] |
|---|---|---|---|---|---|
| 2024-T4 | 177.3 | 14.4 | 12 | 436 | 434 |
| 2024-T4 | 177.3 | 18 | 10 | 448 | 442 |
| 2024-T4 | 177.3 | 23 | 8 | 455 | 452 |
| 2024-T4 | 177.3 | 31 | 6 | 462 | 467 |
| 7075-T3 | 208.5 | 14 | 14 | 406 | 411 |
| 7075-T3 | 208.5 | 18 | 11 | 411 | 418 |
| 7075-T3 | 208.5 | 23 | 9 | 419 | 424 |
| 7075-T3 | 208.5 | 31 | 7 | 430 | 446 |

Due to the unknown properties of the epoxy polyamide film, a sensitivity analysis of the model was performed varying both epoxy film properties and aluminum substrate properties. This analysis shows a strong dependence on substrate properties compared to epoxy film properties for the temperature attained under the same flux and time constraints. The results of changing

material, physical and boundary properties are displayed in Table 5-7. The relative thinness of the epoxy polyamide film makes the temperature gradient of the film difficult to see. However, the difference between the film temperature and temperature at the film-substrate interface is noticeable at the angle the plot is displayed (Figure 5-7). These values show a strong dependence of substrate properties on the epoxy-polyamide film's temperature. A point of interest for these results is that due to the larger mass and volume of the substrate the amount of energy it absorbs only changes 3% at the most.

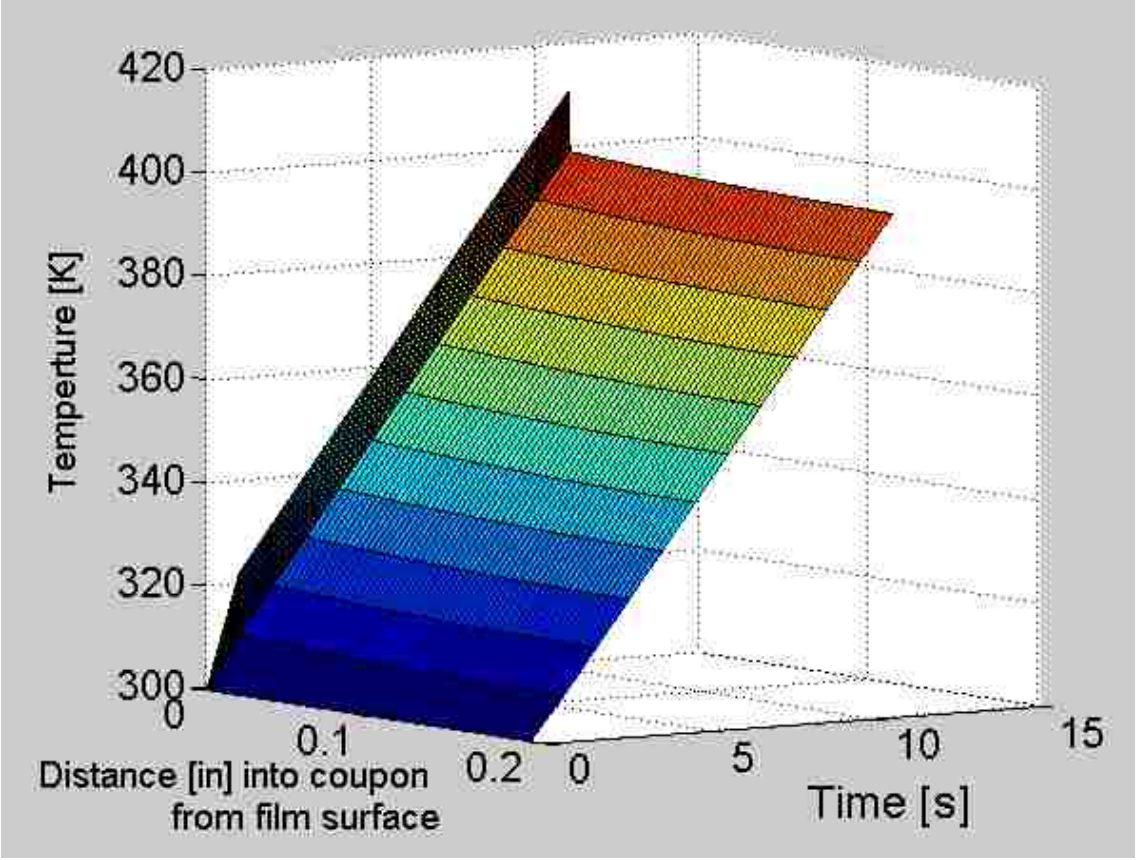


**Figure 5-7: Modeled Coupon Volume Based on Temperature at Nodes for Degradation for a 18 W/cm^2 Incident Flux for 11 seconds of an Epoxy Polyamide Coated 7075 Aluminum Substrate**

The conductivity of the epoxy film had up to a 3.3% effect on surface temperature; a significant contribution considering the film is only 20μm thick. This is due to the already low value of conductivity and doubling or halving the conductive coefficient affects to the films ability to transfer energy. The aluminums conductivity did not have a significant impact on the films absorbed energy only up to 1.7%. This is because of the substrates significantly higher conductivity. The baseline conductivities is about a factor of 500 times in favor of the substrate over the epoxy polyamide. The difference for a short flash did not show a significant change if the ratio of conductivities became 250 or 1000 times greater for the substrate versus than the epoxy film. The response of the temperature to the decreased epoxy conductivity is 3.3% higher temperature at the surface. The energy required for burn initiation is reduced under the lower conductivity. Changing the density or specific heat capacity results in the same magnitude in change of energy absorbed by the epoxy-polyamide primer. If density or specific heat is doubled then the energy absorbed is doubled. This is because the quantity $\rho C_p$ is distributed throughout the heat equation and is equal to the energy of the epoxy polyamide when multiplied by temperature (e.g.$\Delta E = \rho C_p \Delta T$). The energy absorbed is nearly halved or doubled for epoxy primer when the aluminum density and specific heat are varied to half or double the original value. This is because the temperature change in epoxy is affected by the change in energy absorbed by the substrate. The temperature of the substrate increases when the density or specific heat is halved, requiring more of the energy to be absorbed by the epoxy polyamide, but just the opposite for when

the density or specific heat doubles. This shows the dependence on the mass available to store the energy of the film or substrate. The increased thickness of the epoxy polyamide has an additional increase in energy absorbed due to the lower conductivity of the epoxy polyamide. This causes the temperature difference between to film surface and film-substrate interface to be greater for thicker films.

**Table 5-7: Results as Percent Differences of the Modeled Variable Changes Based on the Original Model Conditions and Values**

| | Modeled Temperature %Difference | Modeled Energy Absorbed in Aluminum %Difference | Modeled Energy Absorbed in Epoxy Film %Difference |
|---|---|---|---|
| Epoxy k doubled | -1.2 | 2.2 | -2.1 |
| Epoxy k halved | 3.3 | 1.2 | 6.3 |
| Epoxy ρ or $C_p$ halved | 0.3 | 1.3 | -49.8 |
| Epoxy ρ or $C_p$ doubled | 0.1 | 0.7 | 100.2 |
| Epoxy thickness halved | -1.2 | 1.3 | -51.0 |
| Epoxy thickness doubled | 3.1 | 0.7 | 111.4 |
| Aluminum k doubled | 0.1 | 1.0 | -0.3 |
| Aluminum k halved | 0.5 | 1.4 | 1.7 |
| Aluminum ρ or $C_p$ halved | 26.6 | -1.1 | 90.7 |
| Aluminum ρ or $C_p$ doubled | -13.3 | 2.5 | -46.4 |
| Aluminum thickness doubled | -13.0 | 3.1 | -44.8 |
| Aluminum thickness halved | 26.5 | -1.2 | 90.3 |
| Convection doubled | -0.1 | -0.4 | -1.3 |
| Convection halved | 0.1 | 0.2 | 0.0 |
| Emissivity halved | 0.1 | 0.3 | 0.3 |

The last part of the model that was considered was the boundary condition coefficient values for convection and emissivity. Changing the values at the back surface resulted in very small changes <0.1% and the changes to the back

surface are not displayed in Table 5-7. The changes to coefficients at the film surface resulted in more significant changes; however, these were small compared to changing material properties. The most significant change from boundary conditions comes from doubling the convective coefficient and that resulted in a 1.3% drop in energy absorbed by the epoxy film and a nearly negligible difference in the temperature of the film.

The thicknesses of the two substrates were different for the current experiment. The thickness of the substrate was shown from the modeling to be a significant factor. To eliminate substrate thickness effects the thickness was set equal to 0.125 inches for both substrates. The fluxes and durations of the 2024-T4 experimental values were used in these equal-thickness runs. All other material properties for the substrates remained the same. The absorptivities for the two materials remained at 60% for the 2024-T4 substrate and 65% for the 7075-T3 substrate. The results of such runs showed only a 1% difference for the epoxy polyamide surface temperature. At the end of the duration the epoxy surface temperature was 1% lower for the 7075-T3 substrate because of its higher energy capacity. More energy (5%) was absorbed by the 7075-T3 substrate from the flash as the 7075-T3 aluminum had a higher density and specific heat capacity than the 2024-T4 aluminum. The difference in energies absorbed by the epoxy was within 1% as shown by these equal-thickness calculations. The reason the epoxy film temperature and absorbed energy almost did not with substrate type for these equal-thickness runs is that the 7075-T3 aluminum had a higher absorptivity that was balanced out by the higher density

and specific heat capacity. Using other materials such as steel or different alloys may not have this same temperature or energy profile. The difference in the amount of energy absorbed from the flash for coupons of different materials may cause the results to vary. Experimental verification is needed to determine the correct absorptivity to use when modeling different substrates.

### 5.4 Improvements and Future Work

Future work or improvements for this research include elements of experimentation and knowledge that was not available at the time this research was conducted for the material properties of the epoxy polyamide. The specific heat and the thermal conductivity are required to better model the response of the epoxy polyamide thermal degradation. Byproducts of epoxy polyamide thermal degradation need to be evaluated. From the first coupon used for the verification of the experimental setup, many bubbles under the film surface were observed (Figure 3-1), that were not seen in the samples before phase 1 degradation was complete. Reflectivity of the epoxy-polyamide primer also needs to be determined. Knowledge of how the addition of pigments and substrate affect the absorption are needed for improvements in modeling. The experiment needed a single computer controlling the experiment for synchronized data collection of xenon flash lamp shutter time, thermal camera recording and video recording. For further analysis, reflectivity sensors are required to increase confidence in the phase I degradation temperature and absorbed energy. Thinner substrate in combination with similar substrates to this research should be used to determine the heating rate response of the epoxy-polyamide primer.

Epoxies are thermosetting polymers. Thermosetting polymers are comprised of hydrocarbon chains that are cross-linked. Thermosetting polymers do not melt; instead, they degrade and burn. The cross-linking of the epoxy's molecular chains depends upon the curing process and hardener the epoxy is combined with. The curing time and temperature of the epoxy determine the cross-link density of the epoxy. When cured at a higher temperature for a shorter time period, the epoxy has a decreased cross-link density. The coating process of the epoxy not only has an effect on the cross-linking of the epoxy molecules, but also on the orientation of the molecular chains. Epoxy films may have more of the molecular chains oriented parallel to the plane of the film. Epoxy that is thicker, has molecular chains in a randomly chosen orientation (out of plane). Epoxy film properties may be different from epoxy bulk properties for this reason. Density of an epoxy film may be different than bulk epoxy. Chain orientation may provide different conductivities for the film or bulk epoxy. This issue was not considered in the current work. Epoxy polyamide material properties remain unknown. Epoxy polyamide properties assumed for the following work were approximations based on experimental data and similar epoxy compounds. The model showed an accurate fit to the experimental data.

# 6 Conclusions

This research has demonstrated the heating rate dependency on phase I epoxy polyamide degradation temperature. The required energy for burn initiation of the epoxy polyamide primer is dependent on the ability of the substrate to absorb the transferred energy. This is experiment also showed that there is a constant absorbed energy depending on the substrate used. The total energies per volume required to burn the epoxy polyamide film are determined from the modeling. Degradation energy per volume from the modeling calculations are approximately 220$\frac{J}{cm^3}$ for the 7075-T3 aluminum substrate and 288$\frac{J}{cm^3}$ for the 2024-T4 aluminum substrate. The FTCS model showed that the substrate absorbed a significant amount of the energy form the film. The film had transferred most of the absorbed energy into the substrate at burn initiation. The dependence on substrate properties requires a careful evaluation of the thermal degradation epoxy polyamide primers. The degradation byproducts of epoxy polyamide may counteract the corrosion inhibiting properties that the epoxy polyamide was used to prevent. The thermal response of the epoxy polyamide primer is modeled and verified experimentally. The Forward Time Center Space (FTCS) finite difference method was used to model the heating of the epoxy polyamide due to the reasonable use of computer resources. A parametric analysis of the model showed the dependence on substrate with respect to the measured temperature.

# 7 References

1. *Femtosecond Pulsed Laser Damage Characteristics of 7% Y2O3-ZrO2 Thermal Barrier Coating.* **Das, D.K., et al.** 3, June 1, 2008, Applied Physics A: Materials Science and Prossesing, Vol. 91, pp. 421-428.

2. *Thermal degradation behavior of epoxy resin blended with propyl ester phosphazene.* **Denq, Bar-Long, et al.** 5, 2001, Journal of Applied Polymer Science, Vol. 81, pp. 1161-1174.

3. **Epoxy Technology, Inc.** Epoxy Technology. [Online] 2009. [Cited: May 12, 2012.] http://www.epotek.com/SSCDocs/whitepapers/Adhesive%20Application%20Guide.pdf.

4. ***MIL-PRF-23377K Performance Specification Primer Coatings: Epoxy, High-Solids.*** **June 7, 2012.**

**5. MIL-DTL-81706B. Military Detail Specification (MIL-DTL)-81706B Chemical Conversion Materials for Coating Aluminum and Aluminum Alloys. revision B May 2, 2006. MIL-DTL-81706B.**

**6. *An analytical modeling of heat transfer for laser-assisted nanoimprinting processes.* Hsiao, F. B., et al. s.l. : Springer-Verlag, 2006, Computation Mechanics, Vol. 37, pp. 173-181.**

**7. *Laser-induced damage in cold-sprayed composite coatings.* Rolland, G., et al. 21-22, August 26, 2011, Surface & Coatings Technology, Vol. 205, pp. 4915-4927.**

**8. Griffis, C. A., Masumura, R. A. and Chang, C. I. *Thermal Response of Graphite Epoxy Composite Subject to Rapid Heating.* Washington D.C. : Naval Research Laboratory, 1981.**

**9. *An Investigation of the Thermal Degradation of Epoxy Maleate of Bisphenol A.* Rosu, Dan, et al. July 29, 2004, Journal of Analytical and Applied Pyrolysis, Vol. 72, pp. 191-196.**

**10. *Interaction of Beam and Coated Metals at High Power Continuous Irradiation.* Kim, Yong Hyeon, Baek, Won-Kye and Yoh, Jack J. March 18, 2011, Optics and Lasers in Engineering, Vol. 49, pp. 780-784.**

**11. *Experimental Study and Numerical Simulation of Epoxy Intumescent Passive Fire Protection Performance.* Mercedes, Gómez-Mares, et al.**

**12. Çengel, Yunis A. *Heat and Mass Transfer: A Practical Approach.* 3rd. Pennsylvania State University : McGraw-Hill, 2007.**

**13. Heinrick, Juan C. and Pepper, Darrell W. *Intermediate Finite Element Method: Fluid Flow and Heat Transfer Applications.* Philadelphia : Taylor & Francis, 1999.**

**14. McMaster-Carr. [Online] McMaster-Carr, May 23, 2012. [Cited: May 23, 2012.] http://www.mcmaster.com/#standard-aluminum-sheets/=moe3zi.**

**15. *Thermal Properties of Epoxy (DGEBA)/Phenolic Resin (NOVOLAC) Blends.* Ali, Shokralla Sammani and Al-Muaikel, Nayef Saleh. 1B, 2010, The Arabian Journal for Science and Engineering, Vol. 35, pp. 7-14.**

**16. Montgomery, Douglas C. *Design and Analysis of Experiments.* 6th. Phoenix : John Wiley & Sons, Inc., 2005.**

**17. *Solar spectral optical properties of pigments—Part II: survey of common colorants.* Levinson, Ronnen, Berdahl, Paul and Akbari, Hashem. 4, 2005, Solar Energy Materials and Solar Cells, Vol. 89, pp. 351-389.**

**18. *Transient Heat Transfer Analysis of Functionally Graded Materials Using Adaptive Precise.* Biaosong, Chen, et al. 2, 2004, Numerical Heat Transfer, Part B: Fundamentals: An International Journal of Computation and Methodology, Vol. 45, pp. 181-200.**

**19. *Analysis of transient heat transfer in multilayer thin films with nonlinear thermal boundary resistance.* Ramadan, K. and Al-Nimr, M.A. 2009, International Journal of Thermal Sciences, Vol. 48, pp. 1718-1727.**

**20. *Interaction of Beam and Coated Metals at High Power Continuous Irradiation.* Yong, Hyeon, Kim, Won-Kye, Baek and Jack, J.Yoh. March 18, 2011, Optics and Lasers in Engineering, Vol. 49, pp. 780-784.**

**21. Doron, Bar-Shalom. *Altitude Effects on Heat Transfer Processes in Aircraft Electronic Equipment Cooling.* Cambridge : Massachusettes Insitute of Technology, 1989.**

**22. *Thermal properties of siliconized epoxy interpenetrating coatings.* Kumar, Ananda S and Narayanan, Sankara T.S.N. 2002, Progress in Organic Coatings, Vol. 45, pp. 323-330.**

**23. *Kinetics Study on Thermal Decomposition of Resin Systems.* Wang, Jiangbo, et al. 8, 2012, Journal of Macromolecular Science, Part B: Physics, Vol. 51, pp. 1525-1536.**

**24. *Effect of UV Illumination on Surface Flashover Characteristics of Epoxy Resin under Pulse with Nanosecond Rise Time in Vacuum.* Wang, Zeng-Bin, Cheng, Yong-Hong and Wu, Kai. 2, 2011, IEEE Transactions on Dielectrics and Electrical Insulation, Vol. 18, pp. 561-569.**

**25. StatTrek.com. StatTrek: Teach Yourself Statistics. [Online] StatTrek, 2013. [Cited: January 22, 2013.] http://stattrek.com/.**

**26. *Morphology, flexural, and thermal properties of sepiolite modified epoxy resins with different curing agents.* Nohales, Andre`s, et al. 2006, European Polymer Journal, Vol. 42, pp. 3093-3101.**

**27. *A Transient Heat and Mass Transfer Model of Residential Attics Used to Simulate Radiant Barrier Retrofits.* Medina, M. A., O'Neal, D. L. and W.D.Turner. Februrary 1998, Journal of Solar Energy Engineering, Vol. 120, pp. 32-38.**

**28. *Cleaning of artificially soiled paper using nanosecond, picosecond and femtosecond laser pulses.* Pentzien, Simone, et al. 2, Berlin/Heidelberg : Springer-Verlag, November 2010, Applied Physics A: Materials Science & Processing, Vol. 101, pp. 441-446.**